Temperature and genetic background drive mobilization of diverse transposable elements in a global human fungal pathogen

Anna I. Mackey[1], Vesper Fraunfelter[1], Samantha Shaltz[1], John McCormick[2], Callan Schroeder[1], John R. Perfect[3], Cedric Feschotte[2], Paul M. Magwene[4], Asiya Gusa[1]

[1]Department of Molecular Genetics and Microbiology, Duke University, Durham, North Carolina, United States of America

[2]Department of Molecular Biology and Genetics, Cornell University, Ithaca, New York, United States of America

[3]Department of Medicine, Duke University, Durham, North Carolina, United States of America

[4]Department of Biology, Duke University, Durham, North Carolina, United States of America

* **Corresponding author**

Email: asiya.gusa@duke.edu

ABBREVIATIONS

5mC – 5-methylcytosine

CMC – CACTA, Mirage, Chapaev

Indel – Insertion-deletion

KDZ – Kyakuja, Dileera, Zisupton

LTR – Long terminal repeat

Rap+FK506 – Rapamycin and FK506

RNAi – RNA interference

SNP – Single nucleotide polymorphism

TSD – Terminal site duplication

TE – Transposable element

TIR – Terminal inverted repeat

ABSTRACT

Transposable elements (TEs) are key agents of genome evolution across all domains of life. These mobile genetic elements can cause mutations through transposition or by promoting structural rearrangements. Stress conditions can amplify TE mobility, either by impairing TE suppression mechanisms or through stress-induced interactions between transcription factors and TE sequences, offering a route for rapid genetic change. As such, TEs represent an important source of adaptability within populations. To investigate the interplay between environmental stress and eukaryotic TE dynamics relevant to infectious disease, we examined how heat stress and host-mimicking medium (RPMI) affect TE mobility in the global human fungal pathogen *Cryptococcus neoformans*, using a collection of clinical and environmental isolates. Using a selection-based screen, we captured the mobilization of seven distinct mobile element families, encompassing diverse retrotransposons and DNA transposons, whose insertions conferred antifungal resistance. This includes a novel element, CNEST, which belongs to the CACTA, Mirage, Chapaev (CMC) supergroup. Heat stress at human body temperature (37°C) significantly increased the mobilization of a subset of these TEs, leading to higher rates of acquired antifungal resistance. Whole-genome assemblies revealed that, compared to retrotransposons, DNA transposons were hypomethylated and approximately uniformly distributed throughout the genome, features that may contribute to their frequent mobilization. We further assessed TE-driven genomic changes within hosts using serial isolates from patients with recurrent cryptococcal infections and from isolates passaged through mice. While we observed evidence of TE copy number changes near chromosome ends, we found no indication of TE-mediated alterations near gene-coding regions across any of the serial isolates. Finally, TE mobility was isolate- and strain-dependent, with significant variation even among clonally related strains collected from the same patient, emphasizing the role of genetic background in shaping TE activity. Together, these findings reveal a complex and dynamic relationship between environmental stress, genetic background, TE type-specific epigenetic regulation, and TE mobility, with important implications for adaptation and acquired antifungal resistance in *C. neoformans*.

AUTHOR SUMMARY

Transposable elements (TEs) are mobile segments of DNA that can “jump” from one place to another in a genome, causing genetic changes that can impact fitness and evolution. In this study, we investigate how different environmental conditions influence TE mobility in the pathogenic yeast *Cryptococcus neoformans*, which is globally distributed in the environment and causes life-threatening infections. We compared genetically diverse strains and found that growth at higher temperatures, specifically human body temperature (37°C), increases the mobility of some TEs. In contrast, other TEs were more active at lower temperatures (30°C), indicating distinct pathways of temperature regulation for different TE groups. By examining *C. neoformans* isolates from patients with recurrent infections, we observed genetic changes by one TE group that likely occurred during infection. We also found that TE groups are distributed differently across the genome and show varying levels of DNA methylation, a modification that can suppress their activity and control TE mobility in the cell. Overall, this work shows that environmental stresses, such as increased temperature, can accelerate genetic change by promoting TE mobilization. These changes may contribute to how *C. neoformans* adapts during infection or in the environment.

INTRODUCTION

Transposable elements (TEs) are powerful drivers of genomic change and provide a mechanism for adaptive evolution in fungal pathogens [1–9]. TEs are mobile genetic elements that fall into two broad categories: retrotransposons, which mobilize via an RNA intermediate through a “copy-and-paste” mechanism, and DNA transposons, which mobilize via a DNA intermediate, typically through a “cut-and-paste” mechanism [10]. TE activity can lead to genomic instability through unchecked transposition or by providing homologous sequences throughout the genome that promote rearrangements [11]. However, TEs can also promote beneficial genetic changes, especially under changing or stressful environmental conditions, by modulating the expression of nearby genes, disrupting endogenous gene functions, or providing beneficial cargo [11–15]. Notably, various stressors can increase TE expression and mobilization rates in fungi [1,5,15–18]. TE-mediated genetic changes have been linked to multiple adaptive phenotypes, including increased fitness under heavy metal stress in *Schizosaccharomyces pombe* and nitrogen-limited conditions in *Saccharomyces cerevisiae* [1–

5]. However, despite the demonstrated influence of TEs on adaptative genomic change, spontaneous transposition events are rarely observed in *S. pombe* and *S. cerevisiae* under many environmental conditions [19–22]. Therefore, the extent to which TEs contribute to the rapid adaptation of yeast to environmental stressors remains an open question.

Diverse TEs are present in *Cryptococcus neoformans*, a pathogenic yeast which primarily causes disease in immunocompromised individuals such as cancer patients, organ transplant recipients, and people living with HIV/AIDS [23–25]. *C. neoformans* is responsible for approximately 147,000 deaths annually and accounts for up to 20% of AIDS-related mortality [26,27]. It is a ubiquitous environmental yeast, and inhalation of spores or desiccated yeast cells can lead to pulmonary infection that may disseminate across the blood-brain barrier, causing cryptococcal meningitis [23]. Approximately 10 – 20% of patients diagnosed with cryptococcal meningitis experience recurrent disease, which can persist for years despite antifungal treatment [28]. In-host microevolution can result in adaptive genetic changes that enhance antifungal resistance, alter virulence traits, or increase overall pathogenicity, contributing to persistent infections and treatment failure [29–32]. Although in-host microevolution influences disease outcomes, the genetic basis of altered virulence traits and antifungal resistance often remains unknown, potentially because short-read sequencing and variant calling, the primary detection methods, are less suited for identifying structural rearrangements and TE polymorphisms [33].

During infection, *C. neoformans* encounters a variety of stressors during the environment-to-host transition. These include shifts in nutrient availability, pH, exposure to reactive oxygen species, and elevated temperature (37°C) [34]. Previous studies in the less pathogenic sister species *Cryptococcus deneoformans* have shown that heat stress significantly increases TE mobilization rates, exceeding those of single nucleotide polymorphisms (SNPs) and insertions/deletions (indels) by more than threefold per generation during in vitro passaging at 37°C [35,36]. These findings suggest that in stressful environments, TEs can be the primary drivers of genomic change. Indeed, TE mobilization in *C. deneoformans* has been observed during murine host infection and, in both *C. neoformans* and *C. deneoformans*, has been linked to the development of resistance to 5-fluorocytosine (5-FC), a first-line antifungal treatment [35–37]. A prior study in *C. neoformans* assessed whether heat stress increases mutation rates in the reference strain H99 and two additional clinical isolates, finding no association between heat stress and elevated mutation rates [38]. However, given the small number of isolates examined, it remains unclear whether heat stress can increase TE mobilization rates in *C. neoformans* and

how it may affect mutation rates across additional isolates and lineages. Furthermore, it is unknown whether TEs contribute to genetic changes accumulated during persistent human infection in *C. neoformans*, which causes approximately 95% of cryptococcal infections [39].

C. neoformans is known to harbor a variety of TEs, including DNA transposons as well as long terminal repeat (LTR) and non-LTR retrotransposons [24,25]. Due to significant diversity within TE sequences, structures, and mobilization mechanisms, TEs are further subdivided using a hierarchical classification system [40]. TE orders (e.g., LTR) are subdivided into superfamilies (e.g., Ty1/Copia) based on defining structural or sequence features. For instance, DNA transposons that mobilize via a cut-and-paste mechanism typically contain a conserved DDE or DDD catalytic domain within the transposase, which can be used for identification [41]. To date, only a subset of TEs in *C. neoformans* have been classified to the superfamily level, including DNA transposons belonging to the Kyakuja/Dileera/Zisupton (KDZ) and HARBINGER superfamilies, and LTR retrotransposons from the Ty1/Copia and Ty3/Gypsy superfamilies [37,42,43]. Refining TE classification can provide insights into the mechanisms by which stress influences TE mobilization and genome evolution.

Because uncontrolled TE activity can cause genome instability, hosts have evolved mechanisms to suppress their mobilization [44–47]. The best-characterized TE suppression system in *C. neoformans* is RNA interference (RNAi). Through this pathway, transcripts targeted for silencing are processed into small interfering RNAs, which are loaded into the RNA-induced silencing complex to target homologous transcripts for degradation [43,48–50]. RNAi has been shown to silence double-stranded RNAs, transcripts with sub-optimal splicing signals, repetitive transgenes, and TEs in *C. neoformans* [38,43,48,50]. Unlike in the yeast *S. pombe*, RNAi is strictly involved in post-transcriptional silencing in *C. neoformans* and does not lead to transcriptional silencing by facilitating the assembly or maintenance of heterochromatin [43]. Prior studies have shown that loss-of-function mutations in key RNAi genes can lead to a hypermutator phenotype, driven by rampant TE mobilization, but only in strains with high TE burden [37,38]. TE mobilization may also be shaped by epigenetic context. LTR and non-LTR elements are enriched in centromeric and subtelomeric regions [38,42], where they co-localize with epigenetic features of silent chromatin, such as 5-methylcytosine DNA methylation and repressive histone modifications, including H3K27me3 and H3K9me2 [38,42,51–53]. These marks are also enriched in centromeric and subtelomeric regions, and are rarely detected in gene-rich chromosomes arms [38,42,51–53]. Despite this association, the regulatory effects of

155 DNA methylation and heterochromatin on TEs in *C. neoformans* remain poorly understood,
156 particularly regarding their influence on the mobilization of active TE families.

157 In this study, we investigated how infection-associated stressors, including elevated
158 temperature and exposure to a host-mimicking medium (RPMI), influence TE mobilization in *C.*
159 *neoformans*. Using a reporter gene-based approach, we examined TE mobility in genetically
160 diverse clinical and environmental isolates, including representatives from three of the four
161 major lineages (VNI, VNII, and VNBII) [54]. We found diverse, active TEs in *C. neoformans*,
162 including several whose identity or mobility were previously unknown. TE mobility was
163 temperature-dependent for all elements assessed, with heat stress significantly increasing
164 transposition rates for a subset of elements. De novo telomere-to-telomere genome assemblies
165 were used to examine TE-driven genetic changes in serially collected isolates from patients with
166 recurrent cryptococcal meningitis. Using these assemblies, we annotated TEs to assess the
167 genomic distribution and DNA methylation status of various transposable element types. DNA
168 transposons were approximately uniformly distributed throughout the genome and had
169 significantly reduced levels of DNA methylation compared to retrotransposons. Lastly, we found
170 that TE copy number and mobility were highly isolate- and strain-dependent, suggesting that
171 genetic background is a major determinant of TE-mediated genomic impacts. Together, these
172 results highlight the critical roles of environmental factors, particularly temperature, in driving
173 stress-induced genomic changes and adaptive evolution via transposition in the human fungal
174 pathogen *C. neoformans*.

175

176 **RESULTS**

177 **Diverse transposable elements mobilize in a subset of *C. neoformans* clinical isolates**

178 To investigate transposable element (TE) mobilization dynamics in *Cryptococcus*, we
179 obtained a set of 33 clinical isolates from 18 South African patients with recurrent cryptococcal
180 meningitis, collected as part of the GERMS-SA surveillance study (Table S1) [55]. Isolates were
181 collected by plating cerebrospinal fluid on non-selective medium and selecting a single colony at
182 the time of diagnosis (incident) and after subsequent disease relapse(s), which occurred 57 –
183 238 days later, depending on the patient (Fig 1A, Table S1). Using short read sequencing, a
184 prior study confirmed that isolates collected from the same patient differed by few single
185 nucleotide polymorphisms (SNPs) and insertions/deletions (indels), and that these isolates
186 formed monophyletic clades in phylogenetic analyses, suggesting that disease relapses were

187 clonal and not due to reinfection [29]. This set of clinical isolates is genetically diverse, including
188 *Cryptococcus neoformans* isolates belonging to three of the four major clades, VNI, VNII, and
189 VNBII, and *Cryptococcus gattii* isolates belonging to clades VGI and VGIV (Table S1) [54,56].

190 Prior work from our group showed that growth at 37°C increased TE mobilization rates in the
191 less pathogenic species *Cryptococcus deneoformans* [35,36]. To investigate TE mobility under
192 heat stress in *C. neoformans* and *C. gattii*, both recognized as priority fungal pathogens by the
193 World Health Organization [57], we conducted a preliminary screen using a "transposon trap"
194 assay that detects mutations in the ~934 bp *FRR1* (CNAG_03682) reporter gene, a system
195 previously used by our group and others [35,37,38]. Only mutations in *FRR1*, which encodes
196 the shared drug target of the antifungals rapamycin and FK506 (rap+FK506), can confer
197 resistance to both antifungals (Fig 1B) [58]. While mutations in other genes can confer
198 resistance to rapamycin or FK506 individually, rap+FK506 resistance during a short growth
199 period is most likely caused by a mutation in *FRR1*. This selection-based assay facilitates
200 assessment of TE activity by requiring mutation analysis at only one locus. For the preliminary
201 screen, incident and relapse isolates from the 18 South African cases, as well as the reference
202 strain H99, were cultured in non-selective, nutrient-rich YPAD medium at 37°C and plated on
203 medium containing rap+FK506 (Fig 1B). From a total of 37 isolates, ten independent rap+FK506
204 resistant mutants were collected per isolate, yielding 370 independent mutants. The *FRR1* gene
205 was PCR amplified for each independent mutant to determine the causative mutation of drug
206 resistance. Large DNA insertions, approximately 150 bp – 11 kb, detected by PCR amplification
207 and indicative of TE insertions were confirmed by sequencing. Isolates from three of the 18
208 cases screened contained TE insertions disrupting the *FRR1* locus at 37°C: cases 7, 15, and
209 77, which belong to the VNBII, VNI, and VNII clades, respectively (Table 1). Isolates from these
210 three cases were selected to assess the impact of temperature on drug resistance rates and TE
211 mobility. TE mobilization was detected exclusively in *C. neoformans*; of the three *C. gattii* cases
212 screened, only point mutations were identified in *FRR1*. Additionally, no TE insertions were
213 identified in H99, consistent with prior studies [38]. Subsequent screening of rap+FK506-
214 resistant mutants from cases 7 and 77 following growth at 30°C (see below) revealed additional
215 mobile element families.

216 **Table 1. Cases used for in-depth profiling of the impact of temperature on TE mobility,**
217 **whole-genome assembly, and TE mapping.**

Case	Collection Point	Clade	Days After Incident Isolate Collection	TEs identified inserting in *FRR1* in YPAD
7	Incident	VNBII	-	TCN3
7	Relapse	VNBII	137	TCN3, CNL1, KDZ2, KDZ3
15	Incident	VNI	-	CNIRT6
15	Relapse	VNI	166	CNIRT6
15	Relapse 2	VNI	223	CNIRT6
77	Incident	VNII	-	CNEST, KDZ1
77	Relapse	VNII	182	CNEST, KDZ1
77	Relapse 2	VNII	290	CNEST

In addition to the 370 independent rap+FK506 resistant mutants collected as part of the preliminary screen, we collected additional transposon trap mutants from cases 7, 15, and 77, along with an environmental isolate, for in-depth profiling of the effects of temperature (30°C and 37°C) and RPMI medium on TE dynamics. In total, we examined over 1,000 independent rap+FK506-resistant mutants and identified over 350 independent TE insertion events in *FRR1*. Elements were assigned to known families based on sequence similarity to *C. neoformans* TE family consensus sequences in the Repbase TE database, or to GenBank submissions when family-level consensus sequences were unavailable. Family membership was assigned based on the 80-80-80 rule: nucleotide similarity had to exceed 80% over at least 80 base pairs and cover at least 80% of the recovered sequence length [40]. An exception to this was the non-LTR retrotransposon CNL1, which shares only ~60% nucleotide similarity with the CNL1 consensus sequence in Repbase. However, it exhibits high (> 99%) nucleotide similarity to an active mobile element previously classified as CNL1 in *C. neoformans* by Priest et al. (2022), so we have retained this name. In total, we identified seven diverse TE families mobilizing in *C. neoformans* clinical isolates (Fig 1C, Table 1). This includes an element belonging to a family that, to our knowledge, has not been identified in previous studies (CNEST), as well as elements not previously reported to be mobile (CNIRT6, TCN3, KDZ3) (Fig 1C, Table S2). These elements included DNA transposons, as well as long terminal repeat (LTR) and non-LTR retrotransposons.

CNIRT6 transposition drives increased drug resistance rates at 37°C in case 15

239 To assess how heat stress impacts rap+FK506 drug resistance rates, fluctuation assays
240 were performed on case 15 incident, relapse, and relapse 2 isolates. For all fluctuation assays,
241 cultures were grown to saturation at 30°C or 37°C and the average cell population for each
242 isolate and temperature condition was determined to ensure that differences in growth rates did
243 not affect mutation rate estimates. All case 15 isolates displayed significant increases in
244 rap+FK506 resistance rates during growth at 37°C compared to 30°C in YPAD medium, as
245 indicated by non-overlapping 95% confidence intervals (21-, 12-, and 4-fold, respectively) (Fig
246 2A). The spectrum of mutations in *FRR1* was obtained by sequencing the *FRR1* locus of
247 independent mutants, followed by mapping to the wild-type *FRR1* sequence for each isolate
248 (Fig S1A). In cases where sequencing across the locus proved unsuccessful, junction PCR
249 using TE-specific primers was used to determine the mutation type. Strikingly, many of the
250 mutations in *FRR1*, up to 91% in the incident isolate at 37°C, were caused by insertions of a
251 large (~7.5 kb) DNA transposon with 99.7% nucleotide similarity to a putative element named
252 CNIRT6 (GenBank: JQ277267.1) (Fig 2B). CNIRT6 was originally identified in *C. neoformans*
253 strain JF289 through sequence analysis, however, this transposon has not been described in
254 the literature and is absent from TE databases. Mapping of a subset of these insertions
255 revealed CNIRT6 transposition into *FRR1* introns and exons, resulting in 3 bp terminal site
256 duplications (TSDs) with variable sequences (Fig S2A, B). CNIRT6 insertion rates were
257 significantly higher at 37°C compared to 30°C, increasing by 28-, 20-, and 16-fold in the
258 incident, relapse, and relapse 2 isolates, respectively (Fig 2C). Notably, drug-resistance rates at
259 37°C and CNIRT6 mobility at both temperatures decreased progressively in relapse isolates
260 collected 166 and 223 days after the incident isolate.

261 Given the significant differences in CNIRT6 mobilization rates among case 15 isolates, we
262 hypothesized that inter-isolate variability may be driven by differences in copy number, genomic
263 position, or epigenetic regulation. To investigate these factors, and to assess all inter-isolate
264 polymorphisms caused by mobile elements, we performed long-read sequencing to generate
265 contiguous, telomere-to-telomere genome assemblies for the wild-type case 15 incident,
266 relapse, and relapse 2 isolates, which were polished with Illumina reads (Table S3). 5-
267 methylcytosine (5mC) DNA methylation was identified using Nanopore signal data. Given that
268 all CNIRT6 insertions into *FRR1* appeared to be the same length by gel electrophoresis and
269 shared high nucleotide similarity to one another (> 99%), the full-length CNIRT6 sequence,
270 obtained from an insertion into *FRR1*, was used as the query in BLAST-like alignment tool
271 (BLAT) [59] homology searches against case 15 genome assemblies to identify full-length
272 copies (Fig S1A). For all BLAT homology searches predetermined cutoffs of nucleotide identity ≥

273 90% and coverage ≥ 95% were used to call full-length copies. This analysis revealed two full-
274 length CNIRT6 copies that are positionally conserved between incident and relapse isolates:
275 one is an exact match to the CNIRT6 sequence identified inserting into *FRR1*, and the second
276 differs by a single nucleotide substitution (Fig 2D). The nucleotide sequences of both CNIRT6
277 copies are identical between the incident, relapse, and relapse 2 isolates. No DNA methylation
278 was detected in any full-length CNIRT6 copies across all case 15 isolates, as indicated by
279 methylation frequencies < 0.75 at each CpG site, meaning fewer than 75% of long-read signal
280 data supported a methylated call (Table S4). Therefore, differences in genomic copy number,
281 chromosomal location, or DNA methylation do not appear to underlie differences in CNIRT6
282 mobilization rates between serial isolates.

283 To further characterize the active DNA transposon CNIRT6, we performed sequence
284 analysis and found that this element was ~7.5 kb in length and contained 24 bp terminal
285 inverted repeats beginning with 'CACTG' (Fig 1C, Table S2). Though no CNIRT6 movement has
286 been reported in the H99 reference strain, a homology search revealed two approximately full-
287 length copies in H99 (identity ≥ 90% and coverage ≥ 95%), containing a ~6.9 kb gene
288 annotation (CNAG_01367). Repeat masking of the predicted protein sequence to assess
289 similarity to known TEs using Repbase CENSOR revealed hits to transposases from TEs in the
290 CACTA (also known as EnSpm) superfamily, which contain a 'CACTA' motif at their distal ends,
291 resembling the 'CACTG' motif found in CNIRT6 [60]. To confirm that CNAG_01367 encodes a
292 transposase and refine this classification, a multiple sequence alignment was performed using
293 the amino acid sequences from CNAG_01367 and transposases from several cut-and-paste
294 DNA transposons from the CMC (CACTA, Mirage, Chapaev) supergroup [41]. This alignment
295 revealed a conserved DDE motif, which catalyzes the cut-and-paste mechanism of
296 transposition, indicating that CNIRT6 represents a full-length element predicted to encode a
297 transposase of the CMC supergroup (Fig S3A). To examine the relationship of CNIRT6 to other
298 CMC transposons, an unrooted tree was constructed using transposase amino acid sequences
299 representative of CMC families from animals, plants, and fungi. CNIRT6 formed a statistically
300 supported clade (Bootstrap value 79%) with CACTA elements previously identified in other
301 fungi, as well as plants and animals (Fig S3B). We conclude that CNIRT6 is a member of the
302 CACTA superfamily within the CMC supergroup.

303 To comprehensively assess all genomic changes between case 15 isolates that may have
304 been mediated by TEs other than CNIRT6, we performed synteny and read depth analyses, and
305 used Synteny and Rearrangement Identifier (SyRI) [61], to define structural rearrangements and

306 identify insertions, deletions, and duplications. We repeat masked insertions, deletions, and
307 duplications, which revealed no evidence of transposition events between serial isolates, as
308 indicated by the absence of sequence similarity to contiguous full-length TEs and transposition
309 signatures such as TSDs. Relative to the genome reference strain H99, all three case 15
310 isolates contain a segmental duplication of ~614 kb of the left arm of chromosome 5 and a
311 translocation between chromosomes 4 and 14 where the breakpoint lies in the predicted
312 centromeres (Fig 2D). When comparing the case 15 isolates to one another, we identified an
313 inversion of ~1.26 Mb on chromosome 3 present in both the relapse and relapse 2 isolates, and
314 a translocation between chromosomes 1 and 9 present only in the relapse 2 isolate (Fig 2D).
315 Breakpoints for both inter-isolate rearrangements were outside of the predicted centromeres. No
316 TE annotations were observed near rearrangement breakpoints, suggesting that another source
317 of sequence homology or homology-independent DNA repair mechanisms mediated these
318 rearrangements.

319 Lastly, given the robust activity of CNIRT6 in case 15 isolates grown in YPAD, we
320 hypothesized that CNIRT6 may have mobilized during recurrent infections associated with other
321 cases. To test this, we performed Southern blots on a subset of cases to identify putative
322 transposition events between incident and relapse isolates. We generated a 551 bp CNIRT6-
323 specific probe and utilized a restriction enzyme that cuts once within CNIRT6, outside of the
324 probe site, and produces a range of fragment lengths separable by gel electrophoresis (Fig
325 S4A). Consistent with whole-genome assembly comparisons, there was no difference in the
326 hybridization band pattern for CNIRT6 among case 15 isolates (Fig S4B). However, several
327 other patient cases displayed differences in CNIRT6 hybridization band patterns among serial
328 isolates (Fig S4B). Case 1 was of particular interest, as it exhibited changes in the molecular
329 weight of three bands, suggesting that these copies may occupy different genomic locations and
330 indicating putative CNIRT6 transposition events between the incident and relapse isolates.

331 To investigate putative CNIRT6 transposition events in case 1 isolates, we generated whole-
332 genome assemblies of the incident and relapse isolates and performed homology searches
333 using full-length CNIRT6 as the query sequence. No full-length copies of CNIRT6 were detected
334 in either genome; an identical number of truncated copies were present at the same genomic
335 locations in both case 1 isolates (Fig S4C). Additionally, repeat masking of insertions, deletions,
336 and duplications revealed no evidence of TE mobilization events between the isolates. To
337 assess whether mutations that altered recognition sites of the restriction enzyme BspEI (which
338 cleaves at the palindromic sequence ‘TCCGGA’) might explain differences in Southern blot

339 banding patterns, we identified the closest BspEI sites upstream and downstream of CNIRT6
340 copies in the genomes. We found three instances where changes in BspEI sites led to the
341 predicted production of CNIRT6-containing fragments of different lengths, which correspond to
342 the observed band pattern differences, highlighting a limitation of this approach in detecting
343 transposition events. Lastly, in the case 1 relapse isolate a translocation was detected between
344 chromosomes 3 and 10, with the breakpoint located outside of the predicted centromere
345 regions. There were no TEs near the breakpoint, suggesting that this rearrangement was not
346 mediated by TE-derived sequence homology.

347 **CNEST transposition drives increased drug resistance rates at 37°C in case 77**

348 For case 77, the relapse, and relapse 2 isolates displayed significant increases in
349 rap+FK506 drug resistance rates during growth at 37°C vs 30°C (Fig 3A). Of mutations in *FRR1*
350 observed after growth at 37°C, 29 – 82% were caused by insertion of a novel DNA transposon,
351 which we named CNEST (*Cryptococcus neoformans* EnSpm-like Transposon; naming rationale
352 described below) (Fig 3B). CNEST insertions appeared identical in length by gel electrophoresis
353 and mapped to introns and exons in *FRR1* (Fig S1B, S5A). Insertions resulted in 2 bp 'TA' TSDs
354 (Fig S5B). CNEST insertion rates were significantly higher for all isolates at 37°C; 22-, 83-, and
355 36-fold in the incident, relapse, and relapse 2, respectively (Fig 3C). The full-length CNEST
356 sequence was ~7.2 kb in length, with 33 bp TIRs beginning with 'CACGG' (Fig 1C, Table S2).

357 Interestingly, we also identified insertions of the DNA transposon KDZ1, recently
358 characterized by Huang et al. 2024, which occurred at a lower frequency and only during growth
359 at 30°C (Fig 3B) [37]. KDZ1 is an ~11 kb element with 241 bp TIRs, and its insertion into *FRR1*
360 resulted in 8 bp TSDs (Fig S5B, Table S2). The KDZ1 putative transposase contains a catalytic
361 core affiliated with the Kyakuja/Dileera/Zisupton (KDZ) superfamily and a predicted Zn-chelating
362 CxC1 domain, both of which have been previously described in fungi (Fig 1C) [62].

363 Assemblies of the case 77 relapse and relapse 2 isolates revealed conserved copy number
364 and position of CNEST and KDZ1 by homology searches (identity ≥ 90% and coverage ≥ 95%)
365 with 4 full-length copies of CNEST and 5 full-length copies of KDZ1 (Fig 3D). No DNA
366 methylation was detected in any CNEST copies, as indicated by methylation frequencies < 0.75
367 at each CpG site from long-read signal data (Table S4). For KDZ1, a single copy contained one
368 methylated CpG in the relapse (Table S4). In the relapse 2, two KDZ1 copies contained one
369 methylated CpG. The additional methylated CpG in the relapse 2 isolate is ~900 bp upstream of

370 the predicted transposase start codon; however, a single methylated CpG seems unlikely to
371 impact transcription of the transposase.

372 To further characterize CNEST, which has not previously been identified as mobilizing in the
373 H99 reference strain, we performed a homology search, which revealed two approximately full-
374 length copies in H99 (≥ 90% identity and ≥ 95% coverage), containing a ~4.4 kb gene
375 annotation (CNAG_05910). Repeat masking of CNEST and the predicted amino acid sequence
376 of CNAG_05910 revealed no hits to TEs or transposases in the Repbase TE database.
377 However, given the identification of CNIRT6 as a member of the CMC supergroup, we predicted
378 that CNEST may also encode a CMC transposase. Multiple sequence alignment of the
379 CNAG_05910 amino acid sequence with transposases of the CMC supergroup revealed a well-
380 conserved DDE catalytic core, confirming CNAG_05910 as a CMC-type transposase encoded
381 within full-length CNEST (Fig S3A). Phylogenetic analysis places CNEST in a distinct clade from
382 CNIRT6, forming part of a strongly supported clade (Bootstrap value 100%) containing
383 unclassified transposases from diverse animals, including a transposase annotated as a CACTA
384 (also known as EnSpm) element in the Pacific oyster (*Crassostrea virginica*) (Fig S3B). This
385 clade is sister to clades of elements containing Chapaev and Mirage transposases from
386 animals, forming a well-supported monophyletic group (Bootstrap value 86%) (Fig S3B). Thus,
387 CNEST encodes a transposase defining a new superfamily within the CMC supergroup that is
388 distinct but most closely related to Chapaev and Mirage superfamilies.

389 Lastly, no major genomic rearrangements were identified between the case 77 relapse and
390 relapse 2 assemblies and no other TE-mediated genomic changes were detected by repeat
391 masking, as all insertions, deletions, and duplications identified showed no significant sequence
392 similarity to known TEs. Although mutation rate and spectra data are provided for the case 77
393 incident isolate, there was some variability in the growth of independent colonies and some
394 inconsistency in mutation rate observed between independent fluctuation assays. The likelihood
395 of genome instability in this isolate led to its exclusion from nanopore sequencing and genome
396 assembly. In summary, two elements mobilized to mediate drug resistance in case 77: KDZ1,
397 which was detected only at 30°C, and CNEST, which mobilized significantly more frequently at
398 37°C and is now characterized as a novel active TE in *C. neoformans* belonging to the CMC
399 supergroup. Note that the KDZ superfamily, to which KDZ1 belongs, is completely distinct from
400 the CMC supergroup, which includes CNEST and CNIRT6.

401 **Diverse TEs drive temperature and strain-specific TE mobilization dynamics in case 7**

402 The case 7 incident isolate displayed a significantly higher rap+FK506 resistance rate
403 following growth at 37°C compared to 30°C, while the relapse isolate showed no significant
404 difference in drug resistance rates (Fig 4A). For the incident and relapse isolates at 37°C, ~30%
405 of mutations in *FRR1* were caused by insertions of the LTR retrotransposon TCN3, with both
406 full-length and solo LTR insertions detected (Fig 4B, Fig S1C). TCN3 is ~6.3 kb in length with
407 606 bp LTRs, and insertion into *FRR1* occurred in introns and exons, resulting in 5 bp TSDs of
408 variable sequence (Fig 1C, Fig S6A, B, Table S2). TCN3 is a member of the Ty3/gypsy
409 superfamily that has been previously characterized [63]. The TCN3 insertion we identified
410 contains a ~4.7 kb open reading frame with apparently intact Pol domains (reverse
411 transcriptase, RNase H, protease, and integrase) (Fig 1C). Although we did not identify a Gag
412 domain, the first 306 amino acids lack recognizable functional domains and correspond to the
413 region that typically encodes Gag in Ty3/gypsy elements [63]. Moreover, the Gag gene is the
414 most variable component of LTR retrotransposons, making it particularly difficult to detect [64].
415 These observations suggest that TCN3 likely represents an autonomous LTR retrotransposon
416 (Fig 1C, Table S2). We recovered no TCN3 insertions at 30°C out of a total of 68 independent
417 mutants screened, suggesting that the element may exclusively mobilize at higher temperatures
418 (Fig 4B).

419 Surprisingly, over 60% of *FRR1* mutations in the case 7 relapse isolate at 30°C were caused
420 by insertions of diverse TEs, including the non-LTR retrotransposon CNL1 and the DNA
421 transposons KDZ2 and KDZ3 (Fig 4B, Fig S1C). In contrast, mutations in the incident isolate at
422 30°C were exclusively SNPs/indels (Fig 4B). The longest CNL1 insertion we identified in *FRR1*
423 was ~3.5 kb in length and contained a ~2.5 kb open reading frame with an apparently intact
424 reverse transcriptase domain (Fig 1C, Fig S1C). This maximum insertion length matches
425 previous reports of CNL1 transposition [38]. CNL1 insertions identified in *FRR1* ranged from 180
426 bp to ~3.5 kb likely due to premature termination of reverse transcription which can occur during
427 target primed reverse transcription (TPRT) [65]. CNL1 insertions occurred in the *FRR1* 5′
428 untranslated region (UTR) and in an exon, and were associated with TSDs of variable length (0
429 – 13 bp), consistent with findings from prior studies (Fig S6A, B) [38]. For KDZ2 (~9.2 kb with
430 139 bp TIRs) and KDZ3 (~10 kb with 169 bp TIRs), insertion into *FRR1* occurred in introns and
431 exons and resulted in 4 – 8 bp TSDs (Fig 1C, Fig S6A, B, Table S2). The internal sequences of
432 KDZ2 and KDZ3 encode putative transposases with KDZ and CxC1 domains (Fig 1C). Although
433 TCN3 and KDZ3 were previously annotated, this study is the first to demonstrate their mobility.

434 Homology searches of case 7 genome assemblies using full-length TE sequences that
435 inserted into *FRR1* as queries revealed conserved copy number and position of full-length
436 TCN3 (2 copies), KDZ2 (2 copies), and KDZ3 (3 copies) between the incident and relapse
437 isolates (Fig 4C). This indicated that the observed KDZ2 and KDZ3 activity in the relapse isolate
438 was not due to an increase in copy number or change in genomic position. Additionally, no DNA
439 methylation was detected on any full-length KDZ2 or KDZ3 copies in case 7 isolates, and no TE
440 sequence polymorphisms were observed between serial isolates (Table S4). We did, however,
441 identify an expansion of CNL1 copies in the relapse isolate, with the number increasing from 16
442 to 39 full-length copies in arrays in the subtelomeres (Fig 4C). CNL1 copies exhibited varying
443 levels of DNA methylation (Fig 4C, Table S4). The expansion in CNL1 copy number may explain
444 the observed CNL1 mobility in the relapse isolate, which was undetected in the incident isolate
445 (Fig 4B). No genomic rearrangements or other TE-mediated changes, including alterations in
446 copy number or position of TCN3 solo LTRs, were identified between the case 7 isolates.

447 Interestingly, we recovered 13 total CNL1 insertions in *FRR1*; however, all full-length CNL1
448 copies in case 7 genome assemblies are located at the ends of incident and relapse
449 chromosome arms, flanked externally by telomeric repeats ("TAACCCCC," or slight variations
450 thereof), consistent with previous reports (Fig 4C) [24,66]. To further characterize CNL1, we
451 performed a phylogenetic analysis of the reverse transcriptase domain from a full-length CNL1
452 insertion in *FRR1*, and the CNL1 consensus sequence from the Repbase TE database. This
453 analysis revealed that CNL1 is more closely related to non-LTR elements of the R2 superfamily
454 (Fig S3C), which are characterized by a single open reading frame and often insert into specific
455 target sequences [67,68], in contrast to other non-LTR retrotransposons such as LINE1
456 elements which have weak target site specificity [69,70]. CNL1 was found to be most closely
457 related to MoTeR, a sequence-specific telomeric-targeting element described in the fungal plant
458 pathogen *Magnaporthe oryzae* (Bootstrap value 100%) [71]. Additionally, we observed similarity
459 in the TSDs between independent CNL1 insertions in *FRR1*, suggesting potential sequence-
460 specific target site preferences for this element (Fig S6A, B).

461 Centromeres in *C. neoformans* are typically enriched for LTR retrotransposons with > 95%
462 of LTR retrotransposons, including TCN3, restricted to centromeric regions in the H99 genome
463 reference strain, though the mechanism or selective pressure driving centromere targeting of
464 insertions remains unclear [42]. Although endogenous TCN3 copies in case 7 isolates are
465 restricted to centromeres, 21 independent TCN3 insertions were detected in *FRR1* (Fig 4B).

466 Mapped insertions occurred at variable sequences and positions within *FRR1*, indicating a lack
467 of strong sequence-specific insertion preference (Fig S6A, B).

468 *C. neoformans* centromeres are also enriched for DNA methylation, which is thought to
469 contribute to repression of TEs present in these regions [51,52]. Therefore, we assessed
470 whether the centromeric copies of TCN3 were methylated. If methylated, demethylation and
471 subsequent derepression of TCN3 under heat stress in vitro might explain the observed TCN3
472 mobility at 37°C in case 7 isolates [72]. We found that the full-length copies of TCN3 in the case
473 7 isolate genomes reside in hypomethylated regions within the predicted centromere region of
474 Chr 3 for the incident and relapse (data for the incident isolate shown) (Fig 4D). While five to
475 seven 5mC DNA methylation marks were observed in full-length TCN3 copies, they are located
476 at the end of the 3' LTR (Fig 4D, Table S4). This region is not typically transcribed, making the
477 observed DNA methylation unlikely to impact TCN3 transposition [73]. This suggests that loss of
478 DNA methylation at full-length TCN3 copies is unlikely to explain the differential activity of TCN3
479 observed in vitro, where transposition occurred only at 37°C.

480 Our group previously identified the LTR-retrotransposon TCN12 in *Cryptococcus*
481 *deneoformans* as heat stress-activated, mobilizing almost exclusively at 37°C [35,36]. In *C.*
482 *neoformans*, heat shock binding elements (HSEs) in the promoter region of heat-responsive
483 genes have been shown to be bound by the transcriptional activator heat shock factor 1 (Hsf1)
484 during heat stress [74,75]. A putative HSE was previously identified in the TCN12 LTR [36], and
485 upon scanning the TCN3 LTR, we identified two putative HSEs (Fig 4E). This suggests that the
486 elevated mobilization rates of TCN3 and TCN12 at 37°C may result from Hsf1 binding and
487 subsequent upregulation.

488 **TE mobility is altered in RPMI medium**

489 To more closely mimic the environment *C. neoformans* experiences in-host and assess
490 impacts on transposition, we compiled the spectra of mutations in the *FRR1* reporter gene for
491 cases 7, 15, and 77 following growth in chemically defined RPMI tissue culture medium at 37°C
492 [76]. We additionally tested the impact of RPMI medium at 30°C for case 7 isolates given the
493 activity of CNL1, KDZ2, and KDZ3 observed in the relapse isolate at 30°C in YPAD medium (Fig
494 4B). RPMI medium was supplemented with less glucose (0.2%) compared to YPAD (2%) and
495 had a defined starting pH of 7.0. For four of the six isolates, the same TEs were identified as
496 mobile in both YPAD and RPMI medium (Fig S7A, B, C). In case 77 and case 7 incident

497 isolates, CNL1 and KDZ3, respectively, were observed inserting into *FRR1*, events not
498 previously detected in YPAD medium (Fig. S7B, S7C).

499 We next assessed differences in the frequency of TE insertion events between RPMI
500 and YPAD medium. In the case 15 relapse isolate, there was a significant difference in TE
501 insertions into *FRR1*, with fewer insertions occurring in RPMI compared to YPAD at 37°C (two-
502 tailed Fisher's Exact test, p = 5.62e-6) (Fig S7A, Fig 2B). Interestingly, the use of RPMI medium
503 altered TE dynamics in an isolate- and temperature-specific manner in case 7 isolates (Fig S7C,
504 Fig 4B). Differences between RPMI and YPAD medium include: (1) a significant decrease in
505 TCN3 insertions in the relapse at 37°C in RPMI, with no insertions detected (two-tailed Fisher's
506 Exact test, p = 0.00905), (2) a significant increase in KDZ3 insertions in the incident at 30°C in
507 RPMI, with no insertions occurring in YPAD (two-tailed Fisher's Exact test, p = 2.56e-4), and (3)
508 a significant increase in CNL1 insertions in the relapse at 30°C in RPMI (two-tailed Fisher's
509 Exact test, p = 0.0261), highlighting the complex relationship between environment, genetic
510 background, and TE mobility in case 7 isolates. Across all cases assessed, growth in RPMI
511 medium altered either the TE families observed mobilizing or the frequency of insertion events
512 for at least one isolate.

513 **CNEST heat stress-activation is conserved in a geographically and temporally distinct**
514 **environmental isolate**

515 Homology searches revealed full-length CNEST and KDZ1 copies in a previously
516 published *C. neoformans* VNII genome, the same lineage as the case 77 isolates, sequenced
517 from an environmental sample collected from cockatoo droppings in Boston in 2000 (designated
518 cockatoo guano isolate) [31,77]. While the cockatoo guano and case 77 isolates both belong to
519 the VNII clade, they are geographically and temporally distinct, as the case 77 isolates were
520 collected eight years later in South Africa. However, a pairwise whole-genome comparison
521 revealed that the isolates are highly genetically similar, differing by 1,610 SNPs and indels
522 across the genome, corresponding to approximately 0.0085% divergence at the nucleotide
523 level. To better understand mobility of CNEST and KDZ1 in a different strain background, we
524 assessed rap+FK506 drug resistance rates and the spectra of mutations in *FRR1*. Indeed,
525 cockatoo guano isolate drug resistance rates were significantly elevated during growth at 37°C
526 compared to 30°C (Fig 5A). Approximately 20% of mutations in *FRR1* at 37°C were CNEST
527 insertions, while no CNEST insertions were observed at 30°C, strongly supporting that CNEST
528 transposition is induced by heat stress in the cockatoo guano isolate (Fig 5B). To assess the
529 genomic context of CNEST and KDZ1, we performed synteny analysis, which demonstrated

530 that both the copy number and genomic position of CNEST and KDZ1 were conserved between
531 the cockatoo guano and case 77 isolates (Fig 5C). This may suggest that mobilization of
532 CNEST and KDZ1 in the VNII lineage is infrequent in situ, that mobilization events are typically
533 detrimental to fitness, or that there is selective pressure to maintain both the copy number and
534 genomic context of these elements, all possibilities that will require further investigation.

535 Copy number analysis of other mobile TEs identified in this study revealed two full-length
536 copies of KDZ3 in the case 77 genomes and one full-length copy in the cockatoo guano isolate,
537 located at a conserved site shared with one of the case 77 copies (Fig S8A). The second KDZ3
538 copy in the case 77 relapse isolate, located on Chr 12, appears to result from a transposition
539 event, as synteny flanking this copy is maintained between the two isolates and 8 bp TSDs were
540 identified (Fig S8A, B). Repeat masking of insertions and deletions also revealed evidence of an
541 additional TE family, Gypsy-1_CrGa, originally identified in *C. gattii* [78], whose copy number
542 differs between the case 77 relapse and cockatoo guano isolates (Fig S8A). Two Gypsy-1_CrGa
543 transposition events were detected in the cockatoo guano isolate and one in the case 77
544 relapse genome (Fig S8A). All insertions of this element occurred within predicted centromeres
545 and generated 6 bp TSDs of variable sequence (Fig S8B). Other insertions and deletions, which
546 commonly occurred in the centromeres, contained TE sequences but were likely not mediated
547 by transposition, as they involved multiple or fragmented TE copies and lacked transposition
548 signatures such as TSDs. Thus, while KDZ1 and CNEST copy number and position are
549 conserved between these isolates, transposition events involving other TE families have
550 occurred.

551 A recent study passaged the cockatoo guano isolate twice through A/J mice via retro-
552 orbital intravenous injection, collecting a total of ten isolates from the brains and lungs after the
553 second passage [31]. The cockatoo guano isolate was also the point-source isolate for a case
554 of cryptococcal meningitis, from which a single isolate was collected from the patient (PU
555 isolate) [77]. To assess whether transposition of the two highest copy number TEs located
556 outside of the predicted centromeres, CNEST and KDZ1, occurred during murine passage or
557 human infection, we performed Southern analysis using 551 bp CNEST- and 567 bp KDZ1-
558 specific probes on all ten isolates that had undergone two rounds of murine passage, as well as
559 the cockatoo guano and PU isolates. Restriction enzymes that cut once within the TE sequence,
560 outside of the probe site, were used to produce a range of fragment lengths (Fig S9A). The
561 same hybridization band patterns were observed in the original cockatoo guano isolate and in
562 all isolates recovered following infection (Fig S9B, C), indicating that no CNEST or KDZ1

563 mobilization occurred during infection, despite detection of CNEST transposition in vitro at 37°C
564 (Fig 5B). Thus, while heat-stress activation of CNEST appears conserved between
565 environmental and clinical isolates, no transposition events were detected in isolates recovered
566 from human or murine infections.

567 **Full-length copies of TEs are present across multiple isolates and lineages**

568 Because TE mobility was highly isolate- and strain-dependent in the case 15, 77, and 7
569 isolates, where the TEs captured mobilizing were unique to each case, we hypothesized that
570 this may be due to the absence of full-length copies in certain isolate backgrounds. To evaluate
571 the prevalence of full-length TE copies across *C. neoformans* isolates, we conducted homology
572 searches in assembled genomes using the active TE sequences that were identified inserting
573 into the *FRR1* gene as queries. Full-length copies were defined as hits with ≥ 90% nucleotide
574 identity and ≥ 95% coverage of the query sequence. We identified full-length copies of CNIRT6,
575 CNEST, TCN3, KDZ1, and KDZ3 in several genomes of isolates where transposition was not
576 detected using the transposon trap assay (Fig S10A). For example, at least one full-length copy
577 of CNEST was found in all genomes assessed, including strains from the VNI, VNII, and VNBII
578 lineages (Fig S10A). Additionally, while Gypsy-1_CaGr was not observed mobilizing in vitro, at
579 least one full-length copy was present in all genomes, with up to 12 copies detected in the case
580 7 isolates (Fig S10A). While it appears that there may be a link between increased genomic
581 copy number and TE mobility, we do not have sufficient data to formally assess this.

582 To assess whether full-length copies may be present in the 15 *C. neoformans* cases
583 initially screened without available whole-genome assemblies, we performed TE copy number
584 estimation by aligning short reads to representative full-length TE sequences obtained from an
585 isolate in which the TE family was identified as active. Copy numbers were estimated based on
586 normalized read depth, defined as the depth at which ≥ 95% of the TE sequence is covered
587 [37]. This analysis revealed that full-length copies of potentially active elements may be present
588 even in isolates in which no TE mobilization was detected in the preliminary screen, including
589 cases where estimated copy numbers exceeded those in isolates with observed mobilization
590 (Fig S10B).

591 **DNA methylation status may explain differential mobility of TCN3**

592 Although most TEs identified in this study were detected mobilizing exclusively in a
593 single isolate background, additional full-length copies were found in other assemblies or
594 inferred through copy number estimation (Fig S10A, B). This suggests that TE mobility may be

595 differentially regulated across isolate backgrounds. For example, elevated TE mobility in some
596 isolates may be explained by a loss of RNAi functionality or the absence of DNA methylation on
597 TE sequences.

598 To explore potential regulatory mechanisms, we first assessed the levels of DNA
599 methylation in full-length TE copies in which mobilization was either observed or not observed
600 using the transposon trap assay. Full-length TCN3 copies were highly methylated in cases 15
601 and 1, whereas hypomethylated copies were observed in case 7 isolates (Table S4). In contrast,
602 DNA methylation was generally absent from full-length DNA transposons in strains where no
603 mobilization was observed. For example, in whole-genome assemblies, full-length KDZ1, KDZ3,
604 and CNEST elements were unmethylated in isolates where transposition was not observed in
605 *FRR1*, with the exception of CNEST in case 1 (Table S4). These findings suggest that while
606 DNA methylation may play a role in regulating TCN3 mobility at the centromeres, the
607 methylation status of full-length DNA transposons (which are primarily unmethylated) does not
608 explain isolate- or strain-specific differences in mobility.

609 Next, we examined whether genes required for RNAi function were intact in cases where
610 TE mobility was observed. In cases 7, 15, 77, and the cockatoo guano isolate, we first screened
611 for predicted loss-of-function mutations defined as predicted protein sequences < 85% of the
612 expected length using a previously published list of genes essential for RNAi [37]. No genes
613 required for RNAi function exhibited truncated protein sequences. Second, we performed
614 variant analysis and identified zero nonsense or frameshift mutations across the entire coding
615 sequence for RNAi genes in all isolates, providing no strong evidence for loss-of-function
616 mutations.

617 **DNA transposons are predominantly unmethylated and commonly found in gene-rich**
618 **regions**

619 We observed that all full-length, active DNA transposons mapped in the case 15, 77, and
620 7 genomes were located in gene-rich regions along the chromosome arms (Fig 2D, 3D, 4C).
621 This pattern contrasts with the distribution of retrotransposons in *Cryptococcus*, as previous
622 studies have shown that LTR elements predominantly localized in centromeres [42], and non-
623 LTR elements are enriched at chromosome ends [38]. To further investigate the genomic
624 distribution of DNA transposons in *C. neoformans*, which has not previously been described, we
625 took a comprehensive, unbiased approach to assess genome-wide TE content and distribution.
626 De novo TE annotation was performed using the Earl Grey package [79] for cases 1, 7, 15, and

627 77, as well as the genome of the reference strain H99, in which TE mobilization has not been
628 observed unless RNAi is disrupted [38,49]. Results from the first assemblies of serially collected
629 isolates are shown, as assemblies of later relapse isolates from the same patients yielded
630 similar results. TEs occupied approximately 3 – 5% of the genomes analyzed (Fig 6A). While
631 the proportion of LTR retrotransposons remained relatively consistent (2.2 – 2.6%), greater
632 (more than tenfold) variation was observed in the proportion of DNA transposons (0.08 –
633 0.85%), and non-LTR retrotransposons (0.06 – 2.06%) (Fig 6A). Notably, the *C. neoformans*
634 reference strain H99 had the lowest proportion of DNA transposons among all isolates
635 analyzed.

636 To visualize TE distributions, chromosomes were split at the midpoint of the predicted
637 centromere. For each chromosome arm, the length, TE positions, and protein-coding gene
638 annotation positions were scaled from 0 to 1, allowing data from all chromosome arms to be
639 plotted on a single track. In agreement with previously published data, LTR and non-LTR
640 elements cluster in the predicted centromeres and subtelomeres, respectively; these are
641 regions with a lower density of protein-coding genes (Fig 6B). By contrast, DNA transposons
642 appear to be more evenly distributed across chromosome arms (Fig 6B). We used quantile-
643 quantile (QQ) plots to assess whether the positions of DNA transposons along chromosome
644 arms follow a uniform distribution. For each genome, we generated theoretical quantiles as
645 sorted random numbers between 0 and 1; the total number of theoretical quantiles matched the
646 total number of DNA transposon annotations. The plotted points fell approximately along the
647 diagonal of the QQ plots, indicating that DNA transposons were distributed roughly uniformly
648 across the genome (Fig S11).

649 To assess how frequently DNA transposons were methylated, given their presence in
650 gene-rich regions that are not typically methylated in *C. neoformans* [52,53], we compared their
651 5mC DNA methylation levels to those of LTR and non-LTR elements. First, we assessed
652 average methylation density per 100 bp. DNA transposons exhibited significantly lower average
653 5mC densities compared to both non-LTR and LTR retrotransposons (pairwise Wilcoxon rank-
654 sum test with continuity correction; adjusted p values < 2e-16 for both comparisons) (Fig 6C).
655 Additionally, LTR elements exhibited significantly higher DNA methylation densities compared to
656 non-LTR elements (pairwise Wilcoxon rank-sum test with continuity correction; adjusted p value
657 < 2e-16). Second, we assessed the proportion of TE annotations per genome containing at least
658 one high-confidence 5mC call (methylated frequency from nanopore long-read signal data >
659 0.75). According to this analysis, we found that LTR elements are by far the most consistently

660 methylated (55.6 – 71.2% of LTR retrotransposons contained at least one predicted 5mC),
661 followed by non-LTR elements (7.7 – 53.4%), and DNA transposons (5.4 – 15.5%) (Fig S12A,
662 B). The number of methylated LTR and non-LTR retrotransposons was significantly enriched
663 compared to DNA transposons (Fisher's method combined *p* values: 3.2e-64 for LTR elements
664 and 9.2e-19 for non-LTR elements).

665 To estimate background levels of DNA methylation in protein-coding genes, we lifted
666 over gene annotations from the H99 reference genome. The percentage of protein-coding
667 genes with at least one high-confidence 5mC call ranged from 0.5 – 4.5%, indicating that DNA
668 TEs remain significantly enriched for DNA methylation relative to endogenous protein-coding
669 genes (Fisher's method combined *p* value 3.9e-10), albeit at a lower frequency than LTR and
670 non-LTR elements. Thus, the majority of DNA transposons across all genomes analyzed are
671 unmethylated, and those that are methylated exhibit a lower methylation density compared to
672 non-LTR and LTR retrotransposons (Fig 6C, Fig S12A, B). This suggests that DNA methylation
673 is unlikely to play a major role in modulating the activity of DNA transposons in *C. neoformans*.

674

675 **DISCUSSION**

676 Understanding the interplay between mobile genetic elements, environmental stressors,
677 epigenetics, and genetic background is critical for uncovering factors that influence evolutionary
678 rates and the capacity for adaptive change, particularly in the context of fungal pathogens. In
679 this study, we screened a collection of clinical *Cryptococcus* isolates for transposable element
680 (TE) insertions in the *FRR1* reporter gene and profiled rates of rapamycin and FK506
681 (rap+FK506) resistance, as well as mutation spectra, at both 30°C and the heat-stress condition
682 of 37°C. We also generated telomere-to-telomere genome assemblies to assess TE copy
683 number, genomic position, and DNA methylation status in isolates from patients with recurrent
684 cryptococcal infections.

685 ***C. neoformans* hosts diverse active transposable elements**

686 We identified seven TE families mobilizing to confer rap+FK506 resistance, including
687 both retrotransposons (LTR and non-LTR) and DNA transposons (Fig 1). Several of these
688 elements (TCN3, CNIRT6, KDZ3) were not previously recognized as active. In addition, we
689 discovered a novel, active element, which we named CNEST. The diversity of active TEs in *C.*
690 *neoformans* stands in striking contrast to other yeasts commonly used to study TEs, such as

691 *Saccharomyces cerevisiae* and *Schizosaccharomyces pombe*, which harbor only LTR
692 retrotransposons [80,81]. In these species, TE mobilization studies typically rely on TE
693 constructs driven by inducible heterologous promoters, due in part to the low de novo
694 transposition rates of endogenous copies [82–85]. By contrast, in *C. neoformans*, selecting for
695 mutations at a single genomic locus frequently revealed insertions of endogenous TE copies
696 with diverse transposition mechanisms (Figs 2 – 5). The ability to readily capture multiple active
697 TE families mobilizing within a single *C. neoformans* strain underscores the value of this
698 genetically tractable model for studying TE mobilization strategies and regulation in a
699 basidiomycete.

700 Phylogenetic analysis of transposases from CNIRT6 and CNEST revealed that they
701 belong to the CMC supergroup first described by Yuan and Wessler (2011) (Fig S3). However,
702 CNIRT6 and CNEST are only distantly related and fall within two monophyletic clades among
703 CMC elements: one containing CNIRT6 and transposases from plants, animals, and fungi, and
704 a second containing CNEST and transposases from animals and fungi. Thus, *C. neoformans*
705 hosts active members of two different CMC superfamilies, a notable finding given that this group
706 of DNA transposons remains largely understudied in fungi and animals.

707 The use of a single reporter gene to capture TE insertions may have limited our potential
708 for active mobile element discovery, since some TEs have preferences for specific insertion
709 sequences or genetic compartments [11]. However, the *FRR1* reporter system recovered
710 insertions of TCN3 and CNL1, which appear to target centromeric and subtelomeric regions,
711 respectively. Mapping TCN3 insertions in *FRR1* suggested weak sequence specificity (Fig S6).
712 Alternatively, TCN3 insertions may be guided by non-sequence-based features, such as
713 centromere-specific histone variants [86] or heterochromatin-associated proteins [87], or its
714 insertion pattern may be shaped by selective pressures. It remains possible that TCN3 insertion
715 into *FRR1* is relatively rare and that most de novo insertions occur within centromeric regions.

716 CNL1 copies are enriched in subtelomeric regions in case 7 isolates and other *C.*
717 *neoformans* genomes [38]; however, we also recovered insertions of CNL1 within *FRR1* (Fig 4).
718 Phylogenetic analysis revealed that CNL1 is most closely related to R2 elements, and
719 specifically to MoTeR, a telomere-targeting element characterized in the fungal plant pathogen
720 *Magnaporthe oryzae* [71]. Although prior studies have reported that CNL1 preferentially inserts
721 into copies of itself within arrays near telomeric repeats, its precise sequence specificity remains
722 undefined. Limited mapping of CNL1 insertions into *FRR1* reveled that TSDs contained the
723 sequence 'CACCCCT,' which resembles the *C. neoformans* telomere seed sequence

724 ('AACCCCCT' or similar variants), although interpretation was complicated by premature
725 termination of target primed reverse transcription (TPRT) at different positions within the
726 element (Fig S6). Further work is needed to clarify CNL1's target site specificity, including the
727 extent to which it targets telomeric repeats like MoTeR, inserts into its own sequence, or both.
728 Along with TCN3, these findings highlight open questions about factors driving target site
729 selection and TE distribution across genomic compartments. Intriguingly, stress may be one
730 such factor as nutrient deprivation alters Ty5 phosphorylation, shifting its insertion profile from
731 heterochromatic regions to more broadly distributed sites across the genome [87].

732 Lastly, most observed TE mobilization events were driven by apparently full-length TE
733 copies containing detectable functional domains required for mobilization. Phylogenetic analysis
734 revealed full-length, seemingly intact transposase sequences within mobilized DNA
735 transposons, and functional domains required for mobilization were identified in mobilized TCN3
736 and CNL1. We found no evidence for the mobilization of clearly non-autonomous TE copies
737 (significantly shortened or lacking apparent mobilization machinery). However, we did detect
738 truncated CNL1 insertions, likely resulting from premature termination of TPRT, as well as
739 instances of solo TCN3 LTRs, which likely arose from non-allelic recombination between LTR
740 sequences following TCN3 insertion. This contrasts with other organisms, such as humans,
741 plants, and *Drosophila*, where shortened non-autonomous TEs frequently transpose [88–90].

742 Collectively, we identified seven TE families in *C. neoformans*: DNA transposons from
743 the KDZ superfamily and CMC supergroup, alongside a Ty3/Gypsy LTR element and an R2
744 non-LTR element actively transposing. These TEs employ distinct transposition mechanisms
745 and show preferences for different genomic compartments, revealing a rich "ecosystem" of
746 active TEs within *C. neoformans*.

747 **Transposable element mobilization in *C. neoformans* is strongly influenced by**
748 **temperature**

749 Previous work in *C. deneoformans* demonstrated that heat stress increases TE
750 mobilization [35,36]. While some mobile elements in *C. neoformans* followed this pattern,
751 mobilizing more frequently at elevated temperature, we also uncovered TEs that behave
752 differently. Several elements (CNL1, KDZ1, KDZ3) were found to mobilize exclusively at 30°C in
753 vitro. Others (CNIRT6, CNEST) mobilized at both temperatures, but with higher frequency at
754 37°C. Therefore, by limiting our initial screen to 37°C and examining only ten independent
755 mutants, we may have overlooked strains harboring mobile elements that are active only at

lower temperatures or mobilizing at low frequency. Interestingly, we found completely non-overlapping sets of mobilizing TE families in *C. neoformans* and *C. deneoformans* [35,36]. The discovery of TE families that mobilize more frequently at lower temperatures adds further complexity to this system, suggesting the involvement of multiple TE- or host-specific mechanisms in temperature-regulated mobility in *Cryptococcus*. One such mechanism may involve TCN3 exploiting the host's heat shock response via heat shock elements in its LTR to facilitate mobilization (Fig 1E). While heat shock-induced TE activation via host machinery has been demonstrated in plants and animals [91–93], it remains undescribed in fungi.

Other temperature-dependent effects on TE mobility may result from (1) impacts on functionality of TE-encoded machinery, (2) altered TE suppression, or (3) changes in chromatin accessibility at *FRR1* facilitating transposition. First, Ty1 mobilization in *S. cerevisiae* is most frequent at 22°C and absent above 34°C due to inactivity of the Ty1-encoded protease [94]. Similarly, non-functional TE machinery may explain, for instance, why elements from the KDZ superfamily were only captured mobilizing at 30°C. Second, heat stress can disrupt TE suppression: in *Drosophila*, Hsp70 displaces PIWI-interacting RNA (piRNA) biogenesis factors to the lysosome for degradation, leading to transcriptional activation of TEs [95]. In *C. neoformans*, a recent study found a link between the Calcineurin signaling pathway, which is necessary for growth at 37°C, and RNAi-mediated silencing of a repetitive transgene, suggesting a potential mechanism for altered RNAi function during heat stress [96]. Third, heat stress may increase chromatin accessibility at *FRR1*, facilitating higher TE insertion rates independent of any direct effects on TE suppression or machinery [97,98]. Elucidating the mechanisms underlying differential TE mobilization under heat stress in *C. neoformans* will advance our understanding of the role of TEs in adaptive evolution during infection and in other heat-stress contexts. Additionally, it is likely that other environmental factors impact TE mobilization, given that RPMI medium altered TE dynamics across most strains, although it remains unclear whether this is due to changes in nutrient availability, pH, or other factors (Fig S7). Moreover, although CNL1 mobilization was only observed in vitro at 30°C, it was the sole TE implicated in genomic changes during recurrent cryptococcal infection, highlighting that temperature is not the sole regulator.

DNA transposons are hypomethylated relative to retrotransposons, and are commonly found in gene-rich regions

Given that *C. neoformans* lacks a de novo cytosine DNA methyltransferase, DNA methylation as a TE suppression mechanism is relatively inflexible and unlikely to target newly

789 inserted or unmethylated TE sequences [52]. Despite this, a substantial proportion of TEs
790 exhibit DNA methylation: 55.6 – 71.2% of LTR elements and 7.7 – 53.4% of non-LTR elements
791 (Fig S12). In contrast, DNA transposons are less frequently methylated than retrotransposons,
792 with only 5.4 – 15.5% showing methylation. When methylated, DNA transposons exhibit
793 significantly lower average 5-methylcytosine (5mC) density compared to LTR and non-LTR
794 elements (Fig 6). Nonetheless, DNA TEs are still significantly enriched for DNA methylation
795 compared to protein-coding genes. This reduced level of methylation may contribute to the more
796 frequent in vitro mobilization of DNA transposons observed in this study, where five of the seven
797 mobile elements identified were DNA TEs. Furthermore, full-length DNA transposons are more
798 evenly distributed across the genome and are commonly found within gene-rich regions
799 compared to LTR and non-LTR retrotransposons (Fig 6). As a result, DNA TEs may be more
800 likely to mediate genetic changes that alter the expression or function of protein-coding genes.

801 **Transposable elements provide a mechanism for rapid genetic change and facilitate**
802 **adaptation in *C. neoformans***

803 Growth at mammalian body temperature (37°C) significantly increased the rate of
804 acquired resistance to rap+FK506 in both clinical and environmental isolates (Figs 2–5). In all
805 cases, this effect was driven by elevated TE insertion rates, highlighting the role of TEs in
806 generating adaptive phenotypes such as antifungal resistance. These findings suggest that
807 stress may enhance evolvability within *C. neoformans* populations through bursts of rapid TE
808 mobilization.

809 RNA interference (RNAi) is the primary known mechanism for TE suppression in *C.*
810 *neoformans*, and loss of RNAi function is associated with hypermutator phenotypes driven by
811 uncontrolled TE activity [38]. However, recent work has shown that this is not always the case,
812 as some isolates with loss-of-function mutations in essential RNAi genes maintain low TE
813 burdens and mutation rates [37]. In this study, none of the clinical or environmental isolates
814 profiled harbored predicted loss-of-function mutations in RNAi pathway genes. Nevertheless,
815 isolates from cases 15 and 77 exhibited rap+FK506 resistance rates at 37°C comparable to
816 those observed in hypermutator strains, including the mismatch repair-deficient *msh2Δ* mutant
817 [37,38]. This suggests that, in certain strain backgrounds, heat stress alone can be sufficient to
818 induce a hypermutator-like phenotype through increased TE mobility, even in strains with a
819 relatively low TE burden (e.g., two full-length copies of CNIRT6 in case 15 isolates).

820 When assessing the impact of TEs on in-host microevolution, we observed an expansion
821 of CNL1 copy number in serial isolates collected from a patient with recurrent cryptococcal
822 meningitis, suggesting a role for TE activity in within-host evolution (Fig 4). However, no
823 transposition or TE-mediated genomic changes were detected in other longitudinally sampled
824 clinical isolates or in isolates collected following murine passaging. This may suggest that TE
825 mobilization events are rare in vivo, that TE-mediated changes did not confer a selective in-host
826 growth advantage during infection, or that TE-mediated changes occurred in subpopulations not
827 captured by sampling a single isolate. Previous studies in *C. deneoformans* found evidence of
828 transposition occurring during murine infection [35,36]. In these cases, however, only drug-
829 resistant isolates were selected, requiring that loss-of-function mutations at specific reporter loci
830 had occurred. In contrast, there was no selective pressure for evolved drug resistance or other
831 traits during the recovery of patient and mice isolates examined in this study.

832 **Genetic background influences TE mobility**

833 Telomere-to-telomere genome assemblies revealed that the presence of full-length TEs
834 does not reliably predict their mobilization in vitro. For instance, in clonally related case 7
835 isolates, we observed striking differences in KDZ2 and KDZ3 mobilization at 30°C, despite
836 these elements being present at identical copy number and genomic positions, with identical
837 sequences, and lacking DNA methylation in both isolates. Interestingly, of the two single
838 nucleotide polymorphisms (SNPs) previously identified between case 7 isolates, one was an
839 amino acid substitution in *SET5* (CNAG_03890), a predicted protein lysine methyltransferase
840 [29]. This suggests that alternative epigenetic regulation may be driving differential mobility.
841 Similarly, unmethylated full-length CNEST copies were identified in all assembled genomes
842 except for case 1; however, mobilization was observed only in the case 77 and cockatoo guano
843 isolates. Notably, these isolates had the highest CNEST copy numbers, suggesting that copy
844 number may be positively correlated with increased mobility in vitro. These observations
845 suggest that isolate- and strain-specific TE mobility may be regulated by TE copy number
846 polymorphisms, sequence variation within TEs, differential targeting by RNAi, or genetic
847 variation in host factors that control transposition.

848 Altogether, our findings highlight the complex interplay between genetic background,
849 epigenetics, and environmental conditions in governing TE mobilization, with temperature
850 emerging as a major determinant. Further studies should investigate the extent to which stress-
851 induced transposition generates genetic diversity and whether this diversification drives

852 adaptation to infection-relevant stressors and the repeated emergence of antifungal drug
853 resistance in *C. neoformans*.

854

855 **METHODS**

856 **Strains and growth media**

857 The strains used in this study are listed in Table S1. Strains were grown in YPAD
858 medium (1% yeast extract, 2% peptone, 2% dextrose, 0.025% adenine) with 2% agar added for
859 solid media. For host-mimicking conditions, strains were cultured on RPMI plates containing
860 3.45% MOPS, 0.2% glucose, 2% agar, and 1.04% RPMI 1640 powder (Sigma #R1383).
861 Mutants resistant to rapamycin and FK506 (rap+FK506) were selected for on YPAD plates
862 supplemented with 1 µg/mL rapamycin (LC Laboratories) and 1 µg/mL FK506 (Astellas).

863 **Fluctuation assay and mutation spectra**

864 Cultures were inoculated with independent colonies. Each colony was split into 1 mL
865 cultures of YPAD and grown rotating at 30°C or 37°C for 3 days, allowing all cultures to reach
866 saturation. Cells were pelleted, washed, and resuspended in water. Cells were appropriately
867 diluted, plated on solid YPAD medium, and incubated at 30°C for 3 days. Colony counts were
868 used to calculate colony forming units (CFUs) per culture. The remainder of the culture was
869 plated on two rap+FK506 plates and incubated at 37°C for four days before counting colonies.
870 Total CFUs and rap+FK506-resistant colony counts were used to independently calculate the
871 drug resistance rate for each isolate and temperature using the Fluctuation AnaLysis
872 CalculatOR (FALCOR), applying the Ma-Sandri-Sarkar (MSS) maximum likelihood method [99].
873 For all fluctuation assays a minimum of 23 cultures were used to calculate the drug resistance
874 rate. A single rap+FK506-resistant colony from each culture was selected as an independent
875 mutant for genomic DNA isolation, performed using either in-house reagents or a MasterPure
876 Yeast DNA Purification Kit (VWR #76081-694). A minimum of 24 independent drug-resistant
877 mutants were collected per isolate and temperature for the YPAD mutation spectra analysis.

878 The *FRR1* gene was amplified for Sanger (Azenta) or linear amplicon long-read
879 sequencing (Plasmidsaurus). Amplification of *FRR1* was carried out using a variety of
880 polymerases: MyTaq Mix (Thomas Scientific #C755G91), Apex Taq RED Master Mix (Genesee
881 Scientific #42-138), Platinum SuperFi II PCR Master Mix (ThermoFisher #12368010), Q5 High-
882 Fidelity DNA Polymerase (NEB #M0491S), and LongAmp Taq DNA Polymerase (NEB

883 #M0323S). We often observed “phantom” wild-type–sized secondary bands when amplifying
884 across TEs, which can occur as a PCR artifact when amplifying across long repetitive DNA
885 sequences [100]. In these instances, gel extraction using the Zymoclean Gel DNA Recovery Kit
886 (Zymo Research #D4007) was performed on the higher molecular weight bands, which were
887 then sent for sequencing. For TEs identified as inserting into *FRR1*, junction PCR with primers
888 targeting the internal TE sequence and primers flanking *FRR1* were used to confirm a subset of
889 insertion events, as PCR amplification across long repetitive TE sequences can be difficult
890 [100]. Primers used to amplify *FRR1* and for TE-specific junction PCR are listed in Table S5.

891 Sanger sequencing data were analyzed in SeqMan Ultra 17 or DNASTAR Navigator 17
892 by aligning reads to the wild-type *FRR1* sequence for each isolate. TEs were assigned to
893 families based on the 80-80-80 rule: nucleotide similarity greater than 80%, over more than 80
894 base pairs, covering at least 80% of the recovered sequence length [40]. The TE consensus
895 sequence for TCN3 was obtained from Repbase. For TEs lacking family-level consensus
896 sequences, GenBank submissions were used to assign family membership (GenBank
897 accessions: PQ181658 [KDZ1], PQ181660 [KDZ2], PQ181661 [KDZ3], and JQ277267.1
898 [CNIRT6]). CNL1 family membership was called based on sequence similarity to CNL1 mapped
899 by Priest et al. (2022) in Bt65 and Bt81 genome assemblies (BioProject accession
900 PRJNA749953). Domains were identified within full-length TE sequences using InterPro [101].

901 **RPMI mutation spectra**

902 To generate independent mutants during growth on RPMI medium, a prong-plating
903 procedure was carried out. Single colonies were inoculated in liquid YPAD and grown overnight
904 rotating at 30°C, then cells were washed and diluted in water. A custom tool containing 121 flat-
905 tipped pins was used to transfer approximately ~10^4 cells/pin onto non-selective RPMI plates
906 [102]. To confirm there were no pre-existing mutations, cells were also spotted on rap+FK506
907 plates. Confluent spots of cells on these plates would indicate mutations occurred during the
908 overnight growth in YPAD and prong plating would not be possible to generate independent
909 mutants. If less than 5 colonies appeared on these control plates, experiments were continued.
910 RPMI plates were incubated for 3 days at either 30°C or 37°C. RPMI plates were then replica
911 plated to rap+FK506 plates and incubated at 37°C for 3 days. A single colony was picked from
912 each spot for genomic DNA isolation, followed by *FRR1* amplification and either Sanger
913 sequencing (Azenta) or junction PCR. A minimum of 18 independent drug-resistant mutants
914 were collected per isolate and temperature for the RPMI mutation spectra analysis. *FRR1*

915 amplification, junction PCR, Sanger sequencing data analysis, and TE classification were
916 carried out as described above.

917 **TE insertion rate**

918 TE insertion rate was calculated using the proportion of independent mutants with a
919 given TE insertion multiplied by the drug resistance rate. The 95% confidence intervals (CIs) for
920 proportions were determined using the vassarstats.net proportion CI calculator including
921 continuity correction. 95% CI for TE insertion rates were determined by a method employing the
922 square root of the sum of the squares (using the component 95% CI for rates and proportions)
923 [103].

924 **Transposase and reverse transcriptase protein sequence alignments and phylogenies**

925 Transposase and reverse transcriptase protein sequences were obtained from Yuan and
926 Wessler (2011) for CMC (CACTA, Mirage, Chapaev) related sequences, Repbase consensus
927 sequences (https://www.girinst.org/), and from BLASTp (for translated mRNA sequences) or
928 tBLASTn (for translated genomic sequences) via NCBI (https://blast.ncbi.nlm.nih.gov/Blast.cgi).
929 Protein sequences were aligned using MAFFT (https://www.ebi.ac.uk/jdispatcher/msa/mafft)
930 with the following parameters, protein matrix = BLOSUM62, gap opening penalty = 1.53, gap
931 extension penalty = 0.123, tree rebulding number = 2, max iterations = 2, and FFTS = none.
932 Aligned protein sequences were then used to construct maximum likelihood phylogenies with
933 100 bootstrap replicates using MEGA version 11 [104].

934 **Nanopore sequencing**

935 To extract high molecular weight DNA for library preparation, overnight cultures were
936 grown in 50 mL liquid YPAD shaking at 30°C. Cell were pelleted and lyophilized overnight.
937 Genomic DNA was extracted using a cetyltrimethylammonium bromide (CTAB) extraction
938 method with some modifications [105]. Briefly, cells were lysed by bead beating, and DNA
939 extraction buffer (100 mM Tris-HCl, pH 7.5; 1% w/v CTAB; 0.7 M NaCl; 10 mM EDTA; 1% v/v 2-
940 mercaptoethanol) was added and incubated at 65°C for 30 minutes. Chloroform purification was
941 then performed, and layers were separated by centrifugation. The aqueous layer was isolated,
942 and DNA was subsequently precipitated, washed, and treated with RNase A. Sodium acetate
943 (NaOAc) was then added to a final concentration of 0.6 M, and chloroform purification was
944 repeated. DNA was precipitated again, washed, and spooled to collect high molecular weight
945 DNA.

946 DNA quality was assessed using NanoDrop One A260/A280 and A260/A230 ratios
947 (Thermo Fisher Scientific) and quantified using Qubit dsDNA Broad Range Assay Kit (Invitrogen
948 #Q32850) and the Qubit 4 Fluorometer (Invitrogen). To assess DNA fragment length, clamped
949 homogeneous electric field (CHEF) gel electrophoresis was performed using the CHEF Mapper
950 (Bio-Rad). Libraries were prepared using the SQK-LSK110 or SQK-NBD114.24 and EXP-
951 NBD104 kits and sequenced using the MinION Mk1C following manufacturer's instructions
952 (Oxford Nanopore). Sequencing was performed using the MinKNOW software at the default
953 voltage for at least 48 hours. Basecalling was performed using the latest Guppy software
954 (v7.1.4, v6.3.8, or v6.4.8), or with Dorado (v0.8.1). The specific sequencing kit, flow cell, and
955 basecalling methodology used for each isolate is listed in Table S3.

956 **Genome assembly**

957 Demultiplexing was performed using Guppy (v6.5.7). The Canu (v2.2) genome
958 assembler was used to assemble long reads into contigs, small contigs likely representing
959 mtDNA or contaminants (< 200 kb) were discarded [106]. For the case 15 incident isolate only,
960 assembly was performed by combining outputs from Canu and Flye (v2.9.5) [107]. Genome
961 polishing was performed using long reads generated in this study and short reads available
962 under the SRA umbrella project PRJNA37160 [29]. Long reads were mapped to contigs using
963 Minimap2 (v2.24) followed by Medaka (v1.5.0 or v2.0.1) polishing using the appropriate model
964 [108]. Short reads were mapped to the draft assembly using Bowtie2 (v2.4.4) followed by Pilon
965 (v1.24) polishing, which was performed in five iterations, re-mapping the short reads to each
966 new draft assembly before the next iteration of polishing [109,110]. Canu-corrected Nanopore
967 reads were mapped to the assembly using Minimap2 (v2.24) and coverage was visually
968 inspected in the Integrative Genome Viewer (IGV) [111]. To confirm generation of telomere-to-
969 telomere assemblies, contig ends were inspected for the presence of telomere seed sequences
970 [112]. Assembly breaks at the rDNA locus were artificially merged and separated by 50 Ns.
971 Contigs were oriented to match the first serially collected isolate assembly to produce final
972 nuclear genome assemblies. For each isolate, Canu parameters, polishing specifications, and
973 assembly statistics are provided in Table S3.

974 **DNA methylation detection**

975 5-methylcytosine (5mC) DNA methylation at CpG sites was called using Nanopolish
976 (v0.14.0) or f5c (v1.5) (see Table S3 for isolate-specific details). Minimap2 (v2.24) was used to
977 map long reads to the final nuclear assembly for each isolate. For DNA methylation detection

using f5c, POD5 files were converted to BLOW5 using blue-crab (v0.2.0). The Nanopolish helper script methylation_frequency.py was used to calculate the methylation frequency for CpG sites.

Centromere mapping

Predicted centromere regions were determined using a synteny based approach using the H99 reference genome (GCA_000149245.3) where centromere regions have been experimentally identified [38,42,112]. The 5 kb regions flanking H99 centromeres were used as BLASTn (v2.14.0+) queries against assembled genomes for centromere mapping [113,114].

Full-length TE mapping in assembled genomes

To estimate full-length TE copy numbers from assembled genomes BLAT (v35) and BLASTn (v2.14.0+) were used, full-length TE sequences obtained from linear amplicon long-read sequencing of TE insertions into *FRR1* were provided as queries [59]. Full-length copies were defined as hits with identity ≥ 90% and alignment length ≥ 95% of the query length. For BLAT the -minIdentity=90 specification was used, and pslReps (v469) filtered hits to find the best alignment with a minimum coverage of 95% (-minCover=0.95). BLASTn hits meeting full-length criteria were filtered in R (v4.3.3). In instances were BLAT and BLASTn reported different full-length copy number estimates, the higher estimate was used. Only BLASTn was used to detect copies of CNL1 because BLAT reported overlapping CNL1 copies leading to overestimation, this was not observed for other TEs.

Identification of structural rearrangements and synteny analysis

Whole-genome alignment was performed using Minimap2 (v2.24). Dotplots to visualize primary alignments between assemblies were generated in R (v4.3.3) using pafr (v0.0.2). Synteny and Rearrangement Identifier (SyRI) (v1.6.3) was used to define syntenic regions and structural rearrangements between serial isolates using default parameters [61]. Plotsr was used to visualize syntenic regions [115].

Southern analysis

Genomic DNA was prepared using a CTAB DNA extraction method (described above) and digested with restriction enzymes BspEI, PvuII, or PspXI for CNIRT6, MLDT, and KDZ1, respectively (New England Biolabs) [105]. Digests were run on 0.7% agarose gels at 4°C for approximately 16 h. Fragments from the gel were transferred to a charged nylon membrane (Roche). Target probes were prepared using chemiluminescent DIG-labeling (Roche), see Table

1009 S5 for primers used to amplify probes. Hybridization of the DIG probes (DIG Easy Hyb
1010 Granules, Roche) and detection by chemiluminescence using an anti-DIG antibody (Anti-
1011 Digoxigenin-AP Fab Fragments, Roche) were performed according to the recommended
1012 manufacturer's protocols and imaged on film (Amersham Hyperfilm ECL).

1013 **TE annotation and repeat masking**

1014 Transposon annotation was performed using Earl Grey (v4.1.0) with default parameters
1015 [79]. Insertions, deletions, and duplications identified by SyRI were repeat masked using
1016 Genetic Information Research Institute (GIRI) Repbase CENSOR [78].

1017 **Gene annotation**

1018 Gene annotations were lifted over from the H99 reference genome (GCA_000149245.3)
1019 by Liftoff (v1.6.3) with the -polish flag [116].

1020 **TE copy number estimation using short reads**

1021 TE copy number estimation using short reads was performed as previously described
1022 [37]. Briefly, publicly available short reads (PRJNA37160) were mapped to the H99 reference
1023 genome (GCA_000149245.3) using Minimap2 (v2.24), mosdepth (v0.3.10) was used to
1024 calculate the median read depth in 500 bp non-overlapping windows, the median depth reported
1025 was used for normalization [117]. Short reads were also mapped using Minimap2 to a multi-
1026 fasta containing representative full-length TE sequences identified inserting into *FRR1*.
1027 Mosdepth was then used to produce the cumulative read depth distribution. For each TE, read
1028 depth at 0.95 coverage was normalized by the genome-wide median read depth to estimate full-
1029 length copy number.

1030 **RNAi gene loss-of-function prediction**

1031 Genome feature annotation was "lifted over" from the H99 reference genome (FungiDB
1032 R68) to each isolate-specific genome assembly using the software tool Liftoff (v1.6.3) [116]. The
1033 `-polish` option of Liftoff was employed to re-align exons in cases where the lift-over procedure
1034 resulted in start/stop codon loss or introduced an in-frame stop codon. Based on the polished
1035 lift-over annotation, the AGAT GTF/GFF Toolkit software (https://github.com/NBISweden/AGAT)
1036 was used to predict protein sequences for all annotated genes in each strain-specific assembly
1037 using the `agat_sp_extract_sequences.pl` script. Where multiple protein isoforms are annotated
1038 in the reference genome, predictions were generated for each isoform. For each RNAi-related
1039 gene of interest, the predicted amino acid sequences for each isolate were compared to the

1040 H99 reference genome. Candidate loss-of-function alleles were classified as those encoding
1041 proteins whose predicted length is < 85% of the length in H99.

1042 Variant analysis of RNAi genes was performed by aligning the coding sequence of each
1043 RNAi gene from each isolate's polished genome assembly using the corresponding Liftoff gene
1044 annotation to the H99 reference genome coding sequence using MAFFT (v7.526) [118]. Snp-
1045 sites (v2.5.1) was then used to generate a variant call file, and the impact of variants was
1046 assessed using SnpEff (v5.3a) [119,120].

1047

1048 **DATA AVAILABILITY**

1049 Raw nanopore sequencing reads and whole-genome assemblies generated from
1050 isolates used in this study are available on NCBI's Sequence Read Archive (SRA) under
1051 BioProject PRJNA1222431, accession numbers are listed in Table S3. Full-length TE
1052 sequences identified inserting into *FRR1* were uploaded to GenBank, accession numbers are
1053 listed in Table S2.

1054

1055 **ACKNOWLEDGEMENTS**

1056 We thank Dr. Marco Dias Coelho for training and assistance with de novo genome
1057 assembly. We also thank Dr. Arturo Casadevall for providing the cockatoo guano isolate, as well
1058 as the isolates collected after murine passage. We thank Drs. Joseph Heitman and Jun Huang
1059 for helpful discussions and for sharing unpublished results on KDZ transposons in *C.*
1060 *neoformans*. Finally, we thank Dr. Sue Jinks-Robertson for her advice and discussions during
1061 project conceptualization. The isolates from patients with recurrent cryptococcal meningitis in
1062 this study were collected through GERMS-SA surveillance, provided by Dr. N.P. Govender of the
1063 National Institute for Communicable Diseases, South Africa, and shared by Dr. J. Perfect at
1064 Duke University. We thank members of GERMS-SA, 2005 to 2008, including S. Vasaikar
1065 (Eastern Cape); N. Janse van Rensberg, A. Möller, P. Smith, and A. M. Pretorius (Free State);
1066 K. Ahmed, A. Hoosen, R. Lekalakala, P. P. Sein, C. Feldman, A. S. Karstaedt, O. Perovic, J.
1067 Wadula, M. Dove, K. Lindeque, L. Meyer, and G. Weldhagen (Gauteng); S. Harvey and P.
1068 Jooste (Northern Cape); D. Cilliers and A. Rampe (North West Province); W. Sturm, T. Vanmali,
1069 P. Bhola, P. Moodley, S. Sithole, and H. Dawood (KwaZulu Natal); K. Hamese (Limpopo); K.
1070 Bauer, G. Hoyland, J. Lebudi, and C. Mutanda (Mpumalanga); R. Hoffmann, S. Martin, L.

Liebowitz, and E. Wasserman (Western Cape); A. Whitelaw (Western Cape); A. Brink, I. Zietsman, M. Botha, X. Poswa, M. da Silva, and S. Budavari (Ampath laboratories); C. Heney and J. Smit (Lancet laboratories); M. Senekal (Pathcare laboratories); A. Schuchat and S. Schrag (CDC); K. P. Klugman (Emory); and C. Cohen, L. Dini, L. de Gouveia, J. Frean, S. Gould, K. Keddy, K. M. McCarthy, J. Patel, S. T. Meiring, E. G. Prentice, V. C. Quan, J. Ramalivhana, A. Sooka, A. von Gottberg, and N. P. Govender (National Institute for Communicable Diseases).

COMPETING INTERESTS

The authors have declared that no competing interests exist.

REFERENCES

1. Feng G, Leem Y-E, Levin HL. Transposon integration enhances expression of stress response genes. Nucleic Acids Res. 2013 Jan;41(2):775–789.

2. Esnault C, Lee M, Ham C, Levin HL. Transposable element insertions in fission yeast drive adaptation to environmental stress. Genome Res. 2019 Jan;29(1):85–95.

3. Urquhart AS, Chong NF, Yang Y, Idnurm A. A large transposable element mediates metal resistance in the fungus *Paecilomyces variotii*. Curr Biol. 2022 Mar 14;32(5):937–950.e5.

4. McDonald MC, Taranto AP, Hill E, Schwessinger B, Liu Z, Simpfendorfer S, et al. Transposon-Mediated Horizontal Transfer of the Host-Specific Virulence Protein ToxA between Three Fungal Wheat Pathogens. MBio. 2019 Sep 10;10(5).

5. Hays M, Schwartz K, Schmidtke DT, Aggeli D, Sherlock G. Paths to adaptation under fluctuating nitrogen starvation: The spectrum of adaptive mutations in *Saccharomyces cerevisiae* is shaped by retrotransposons and microhomology-mediated recombination. PLoS Genet. 2023 May 16;19(5):e1010747.

6. Singh NK, Badet T, Abraham L, Croll D. Rapid sequence evolution driven by transposable elements at a virulence locus in a fungal wheat pathogen. BMC Genomics. 2021 May 27;22(1):393.

1099 7. Oggenfuss U, Croll D. Recent transposable element bursts are associated with the
1100 proximity to genes in a fungal plant pathogen. PLoS Pathog. 2023 Feb
1101 14;19(2):e1011130.

1102 8. Lorrain C, Feurtey A, Möller M, Haueisen J, Stukenbrock E. Dynamics of transposable
1103 elements in recently diverged fungal pathogens: lineage-specific transposable element
1104 content and efficiency of genome defenses. G3 (Bethesda). 2021 Apr 15;11(4).

1105 9. Badet T, Tralamazza SM, Feurtey A, Croll D. Recent reactivation of a pathogenicity-
1106 associated transposable element is associated with major chromosomal rearrangements
1107 in a fungal wheat pathogen. Nucleic Acids Res. 2023 Dec 24;

1108 10. Wells JN, Feschotte C. A field guide to eukaryotic transposable elements. Annu Rev
1109 Genet. 2020 Nov 23;54:539–561.

1110 11. Bourque G, Burns KH, Gehring M, Gorbunova V, Seluanov A, Hammell M, et al. Ten
1111 things you should know about transposable elements. Genome Biol. 2018 Nov
1112 19;19(1):199.

1113 12. Gluck-Thaler E, Ralston T, Konkel Z, Ocampos CG, Ganeshan VD, Dorrance AE, et al.
1114 Giant starship elements mobilize accessory genes in fungal genomes. Mol Biol Evol.
1115 2022 May 3;39(5).

1116 13. Baduel P, Sammarco I, Barrett R, Coronado-Zamora M, Crespel A, Díez-Rodríguez B, et
1117 al. The evolutionary consequences of interactions between the epigenome, the genome
1118 and the environment. Evol Appl. 2024 Jul 23;17(7):e13730.

1119 14. Horváth V, Merenciano M, González J. Revisiting the Relationship between
1120 Transposable Elements and the Eukaryotic Stress Response. Trends Genet. 2017
1121 Nov;33(11):832–841.

1122 15. Fouché S, Badet T, Oggenfuss U, Plissonneau C, Francisco CS, Croll D. Stress-Driven
1123 Transposable Element De-repression Dynamics and Virulence Evolution in a Fungal
1124 Pathogen. Mol Biol Evol. 2020 Jan 1;37(1):221–239.

1125 16. Sehgal A, Lee C-YS, Espenshade PJ. SREBP controls oxygen-dependent mobilization of
1126 retrotransposons in fission yeast. PLoS Genet. 2007 Aug;3(8):e131.

1127 17. Paquin CE, Williamson VM. Temperature effects on the rate of ty transposition. Science.
1128 1984 Oct 5;226(4670):53–55.

1129 18. Servant G, Pinson B, Tchalikian-Cosson A, Coulpier F, Lemoine S, Pennetier C, et al.
1130 Tye7 regulates yeast Ty1 retrotransposon sense and antisense transcription in response
1131 to adenylic nucleotides stress. Nucleic Acids Res. 2012 Jul;40(12):5271–5282.

1132 19. Scholes DT, Banerjee M, Bowen B, Curcio MJ. Multiple regulators of Ty1 transposition in
1133 *Saccharomyces cerevisiae* have conserved roles in genome maintenance. Genetics.
1134 2001 Dec;159(4):1449–1465.

1135 20. Hénault M, Marsit S, Charron G, Landry CR. The genomic landscape of transposable
1136 elements in yeast hybrids is shaped by structural variation and genotype-specific
1137 modulation of transposition rate. Elife. 2024 Feb 27;12.

1138 21. Garfinkel DJ, Nyswaner KM, Stefanisko KM, Chang C, Moore SP. Ty1 copy number
1139 dynamics in *Saccharomyces*. Genetics. 2005 Apr;169(4):1845–1857.

1140 22. Esnault C, Levin HL. The Long Terminal Repeat Retrotransposons Tf1 and Tf2 of
1141 *Schizosaccharomyces pombe*. Microbiol Spectr. 2015 Aug;3(4).

1142 23. Lin X, Heitman J. The biology of the *Cryptococcus neoformans* species complex. Annu
1143 Rev Microbiol. 2006;60:69–105.

1144 24. Goodwin TJ, Poulter RT. The diversity of retrotransposons in the yeast *Cryptococcus*
1145 *neoformans*. Yeast. 2001 Jun 30;18(9):865–880.

1146 25. Goodwin TJD, Butler MI, Poulter RTM. Cryptons: a group of tyrosine-recombinase-
1147 encoding DNA transposons from pathogenic fungi. Microbiology (Reading, Engl). 2003
1148 Nov;149(Pt 11):3099–3109.

1149 26. Rajasingham R, Smith RM, Park BJ, Jarvis JN, Govender NP, Chiller TM, et al. Global
1150 burden of disease of HIV-associated cryptococcal meningitis: an updated analysis.
1151 Lancet Infect Dis. 2017 Aug;17(8):873–881.

1152 27. Denning DW. Global incidence and mortality of severe fungal disease. Lancet Infect Dis.
1153 2024 Jul;24(7):e428–e438.

1154 28. Chang CC, Dorasamy AA, Gosnell BI, Elliott JH, Spelman T, Omarjee S, et al. Clinical
1155 and mycological predictors of cryptococcosis-associated immune reconstitution
1156 inflammatory syndrome. AIDS. 2013 Aug 24;27(13):2089–2099.

1157 29. Chen Y, Farrer RA, Giamberardino C, Sakthikumar S, Jones A, Yang T, et al.
1158 Microevolution of Serial Clinical Isolates of *Cryptococcus neoformans* var. *grubii* and
1159 *C. gattii*. MBio. 2017 Mar 7;8(2).

1160 30. Ormerod KL, Morrow CA, Chow EWL, Lee IR, Arras SDM, Schirra HJ, et al. Comparative
1161 Genomics of Serial Isolates of *Cryptococcus neoformans* Reveals Gene Associated With
1162 Carbon Utilization and Virulence. G3 (Bethesda). 2013 Apr 9;3(4):675–686.

1163 31. Sephton-Clark P, McConnell SA, Grossman N, Baker RP, Dragotakes Q, Fan Y, et al.
1164 Similar evolutionary trajectories in an environmental *Cryptococcus neoformans* isolate
1165 after human and murine infection. Proc Natl Acad Sci USA. 2023 Jan
1166 10;120(2):e2217111120.

1167 32. Hu G, Chen SH, Qiu J, Bennett JE, Myers TG, Williamson PR. Microevolution during
1168 serial mouse passage demonstrates *FRE3* as a virulence adaptation gene in
1169 *Cryptococcus neoformans*. MBio. 2014 Apr 1;5(2):e00941–14.

1170 33. Ewing AD. Transposable element detection from whole genome sequence data. Mob
1171 DNA. 2015 Dec 29;6:24.

1172 34. Brown SM, Campbell LT, Lodge JK. *Cryptococcus neoformans*, a fungus under stress.
1173 Curr Opin Microbiol. 2007 Aug 17;10(4):320–325.

1174 35. Gusa A, Williams JD, Cho J-E, Averette AF, Sun S, Shouse EM, et al. Transposon
1175 mobilization in the human fungal pathogen *Cryptococcus* is mutagenic during infection
1176 and promotes drug resistance in vitro. Proc Natl Acad Sci USA. 2020 May
1177 5;117(18):9973–9980.

1178 36. Gusa A, Yadav V, Roth C, Williams JD, Shouse EM, Magwene P, et al. Genome-wide
1179 analysis of heat stress-stimulated transposon mobility in the human fungal pathogen
1180 *Cryptococcus deneoformans*. Proc Natl Acad Sci USA. 2023 Jan
1181 24;120(4):e2209831120.

1182 37. Huang J, Larmore CJ, Priest SJ, Xu Z, Dietrich FS, Yadav V, et al. Distinct evolutionary
1183 trajectories following loss of RNA interference in *Cryptococcus neoformans*. Proc Natl
1184 Acad Sci USA. 2024 Nov 19;121(47):e2416656121.

1185 38. Priest SJ, Yadav V, Roth C, Dahlmann TA, Kück U, Magwene PM, et al. Uncontrolled
1186 transposition following RNAi loss causes hypermutation and antifungal drug resistance in
1187 clinical isolates of *Cryptococcus neoformans*. Nat Microbiol. 2022 Aug 2;7(8):1239–1251.

1188 39. Maziarz EK, Perfect JR. Cryptococcosis. Infect Dis Clin North Am. 2016 Mar;30(1):179–
1189 206.

1190 40. Wicker T, Sabot F, Hua-Van A, Bennetzen JL, Capy P, Chalhoub B, et al. A unified
1191 classification system for eukaryotic transposable elements. Nat Rev Genet. 2007
1192 Dec;8(12):973–982.

1193 41. Yuan Y-W, Wessler SR. The catalytic domain of all eukaryotic cut-and-paste transposase
1194 superfamilies. Proc Natl Acad Sci USA. 2011 May 10;108(19):7884–7889.

1195 42. Yadav V, Sun S, Billmyre RB, Thimmappa BC, Shea T, Lintner R, et al. RNAi is a critical
1196 determinant of centromere evolution in closely related fungi. Proc Natl Acad Sci USA.
1197 2018 Mar 20;115(12):3108–3113.

1198 43. Wang X, Hsueh Y-P, Li W, Floyd A, Skalsky R, Heitman J. Sex-induced silencing defends
1199 the genome of *Cryptococcus neoformans* via RNAi. Genes Dev. 2010 Nov
1200 15;24(22):2566–2582.

1201 44. Ilık İA, Yang X, Zhang ZZZ, Aktaş T. Transcriptional and post-transcriptional regulation of
1202 transposable elements and their roles in development and disease. Nat Rev Mol Cell
1203 Biol. 2025 Oct;26(10):759–775.

1204 45. Lisch D. Epigenetic regulation of transposable elements in plants. Annu Rev Plant Biol.
1205 2009;60:43–66.

1206 46. Amselem J, Lebrun M-H, Quesneville H. Whole genome comparative analysis of
1207 transposable elements provides new insight into mechanisms of their inactivation in
1208 fungal genomes. BMC Genomics. 2015 Feb 28;16(1):141.

1209 47. Nicolás FE, Ruiz-Vázquez RM. Functional diversity of RNAi-associated sRNAs in fungi.
1210 Int J Mol Sci. 2013 Jul 24;14(8):15348–15360.

1211 48. Dumesic PA, Natarajan P, Chen C, Drinnenberg IA, Schiller BJ, Thompson J, et al.
1212 Stalled spliceosomes are a signal for RNAi-mediated genome defense. Cell. 2013 Feb
1213 28;152(5):957–968.

1214 49. Burke JE, Longhurst AD, Natarajan P, Rao B, Liu J, Sales-Lee J, et al. A Non-Dicer
1215 RNase III and Four Other Novel Factors Required for RNAi-Mediated Transposon
1216 Suppression in the Human Pathogenic Yeast *Cryptococcus neoformans*. G3 (Bethesda).
1217 2019 Jul 9;9(7):2235–2244.

1218 50. Janbon G, Maeng S, Yang D-H, Ko Y-J, Jung K-W, Moyrand F, et al. Characterizing the
1219 role of RNA silencing components in *Cryptococcus neoformans*. Fungal Genet Biol. 2010
1220 Dec;47(12):1070–1080.

1221 51. Schotanus K, Yadav V, Heitman J. Epigenetic dynamics of centromeres and
1222 neocentromeres in *Cryptococcus deuterogattii*. PLoS Genet. 2021 Aug
1223 31;17(8):e1009743.

1224 52. Catania S, Dumesic PA, Pimentel H, Nasif A, Stoddard CI, Burke JE, et al. Evolutionary
1225 Persistence of DNA Methylation for Millions of Years after Ancient Loss of a De Novo
1226 Methyltransferase. Cell. 2020 Jan 23;180(2):263–277.e20.

1227 53. Dumesic PA, Homer CM, Moresco JJ, Pack LR, Shanle EK, Coyle SM, et al. Product
1228 binding enforces the genomic specificity of a yeast polycomb repressive complex. Cell.
1229 2015 Jan 15;160(1-2):204–218.

1230 54. Desjardins CA, Giamberardino C, Sykes SM, Yu C-H, Tenor JL, Chen Y, et al. Population
1231 genomics and the evolution of virulence in the fungal pathogen *Cryptococcus*
1232 *neoformans*. Genome Res. 2017 Jul;27(7):1207–1219.

1233 55. Van Wyk M, Govender NP, Mitchell TG, Litvintseva AP, GERMS-SA. Multilocus sequence
1234 typing of serially collected isolates of *Cryptococcus* from HIV-infected patients in South
1235 Africa. J Clin Microbiol. 2014 Jun;52(6):1921–1931.

1236 56. Bovers M, Hagen F, Kuramae EE, Boekhout T. Six monophyletic lineages identified
1237 within *Cryptococcus neoformans* and *Cryptococcus gattii* by multi-locus sequence typing.
1238 Fungal Genet Biol. 2008 Apr;45(4):400–421.

1239 57. Antimicrobial Resistance Division (AMR), Control of Neglected Tropical Diseases (NTD),
1240 Global Coordination and Partnership (GCP). WHO fungal priority pathogens list to guide
1241 research, development and public health action. World Health Organization (WHO); 2022
1242 Oct.

1243 58. Cruz MC, Cavallo LM, Görlach JM, Cox G, Perfect JR, Cardenas ME, et al. Rapamycin
1244 antifungal action is mediated via conserved complexes with FKBP12 and TOR kinase
1245 homologs in *Cryptococcus neoformans*. Mol Cell Biol. 1999 Jun;19(6):4101–4112.

1246 59. Kent WJ. BLAT--the BLAST-like alignment tool. Genome Res. 2002 Apr;12(4):656–664.

1247 60. Fedoroff NV. Molecular genetics and epigenetics of CACTA elements. Methods Mol Biol.
1248 2013;1057:177–192.

1249 61. Goel M, Sun H, Jiao W-B, Schneeberger K. SyRI: finding genomic rearrangements and
1250 local sequence differences from whole-genome assemblies. Genome Biol. 2019 Dec
1251 16;20(1):277.

1252 62. Iyer LM, Zhang D, de Souza RF, Pukkila PJ, Rao A, Aravind L. Lineage-specific
1253 expansions of TET/JBP genes and a new class of DNA transposons shape fungal
1254 genomic and epigenetic landscapes. Proc Natl Acad Sci USA. 2014 Feb 4;111(5):1676–
1255 1683.

1256 63. Coffin JM, Hughes SH, Varmus HE. Structural Classes of Retroelements and Replication
1257 Strategies. 1997;

1258 64. Eickbush TH, Jamburuthugoda VK. The diversity of retrotransposons and the properties
1259 of their reverse transcriptases. Virus Res. 2008 Jun;134(1-2):221–234.

1260 65. Cost GJ, Feng Q, Jacquier A, Boeke JD. Human L1 element target-primed reverse
1261 transcription in vitro. EMBO J. 2002 Nov 1;21(21):5899–5910.

1262 66. Priest SJ, Coelho MA, Mixão V, Clancey SA, Xu Y, Sun S, et al. Factors enforcing the
1263 species boundary between the human pathogens *Cryptococcus neoformans* and
1264 *Cryptococcus deneoformans*. PLoS Genet. 2021 Jan 19;17(1):e1008871.

1265 67. Yang J, Malik HS, Eickbush TH. Identification of the endonuclease domain encoded by
1266 R2 and other site-specific, non-long terminal repeat retrotransposable elements. Proc
1267 Natl Acad Sci USA. 1999 Jul 6;96(14):7847–7852.

1268 68. Christensen SM, Ye J, Eickbush TH. RNA from the 5’ end of the R2 retrotransposon
1269 controls R2 protein binding to and cleavage of its DNA target site. Proc Natl Acad Sci
1270 USA. 2006 Nov 21;103(47):17602–17607.

1271 69. Fujiwara H. Site-specific non-LTR retrotransposons. Microbiol Spectr. 2015
1272 Apr;3(2):MDNA3–0001.

1273 70. Jurka J. Sequence patterns indicate an enzymatic involvement in integration of
1274 mammalian retroposons. Proc Natl Acad Sci USA. 1997 Mar 4;94(5):1872–1877.

1275 71. Starnes JH, Thornbury DW, Novikova OS, Rehmeyer CJ, Farman ML. Telomere-targeted
1276 retrotransposons in the rice blast fungus *Magnaporthe oryzae*: agents of telomere
1277 instability. Genetics. 2012 Jun;191(2):389–406.

1278 72. Korotko U, Chwiałkowska K, Sańko-Sawczenko I, Kwasniewski M. DNA Demethylation in
1279 Response to Heat Stress in *Arabidopsis thaliana*. Int J Mol Sci. 2021 Feb 4;22(4).

1280 73. Zhang L, Yan L, Jiang J, Wang Y, Jiang Y, Yan T, et al. The structure and
1281 retrotransposition mechanism of LTR-retrotransposons in the asexual yeast *Candida*
1282 *albicans*. Virulence. 2014 Aug 15;5(6):655–664.

1283 74. Yang D-H, Jung K-W, Bang S, Lee J-W, Song M-H, Floyd-Averette A, et al. Rewiring of
1284 Signaling Networks Modulating Thermotolerance in the Human Pathogen *Cryptococcus*
1285 *neoformans*. Genetics. 2017 Jan;205(1):201–219.

1286 75. Gao X, Fu Y, Sun S, Gu T, Li Y, Sun T, et al. Cryptococcal Hsf3 controls
1287 intramitochondrial ROS homeostasis by regulating the respiratory process. Nat Commun.
1288 2022 Sep 15;13(1):5407.

1289 76. Kang YS, Jung J, Brown HL, Mateusiak C, Doering TL, Brent MR. Leveraging a new data
1290 resource to define the response of *Cryptococcus neoformans* to environmental signals.
1291 Genetics. 2025 Jan 8;229(1):1–29.

1292 77. Nosanchuk JD, Shoham S, Fries BC, Shapiro DS, Levitz SM, Casadevall A. Evidence of
1293 zoonotic transmission of *Cryptococcus neoformans* from a pet cockatoo to an
1294 immunocompromised patient. Ann Intern Med. 2000 Feb 1;132(3):205–208.

1295 78. Kohany O, Gentles AJ, Hankus L, Jurka J. Annotation, submission and screening of
1296 repetitive elements in Repbase: RepbaseSubmitter and Censor. BMC Bioinformatics.
1297 2006 Oct 25;7:474.

1298 79. Baril T, Galbraith J, Hayward A. Earl Grey: A Fully Automated User-Friendly Transposable
1299 Element Annotation and Analysis Pipeline. Mol Biol Evol. 2024 Apr 2;41(4).

1300 80. Kim JM, Vanguri S, Boeke JD, Gabriel A, Voytas DF. Transposable elements and
1301 genome organization: a comprehensive survey of retrotransposons revealed by the
1302 complete *Saccharomyces cerevisiae* genome sequence. Genome Res. 1998
1303 May;8(5):464–478.

1304 81. Levin HL, Weaver DC, Boeke JD. Two related families of retrotransposons from
1305 *Schizosaccharomyces pombe*. Mol Cell Biol. 1990 Dec;10(12):6791–6798.

1306 82. Curcio MJ, Lutz S, Lesage P. The Ty1 LTR-Retrotransposon of Budding Yeast,
1307 *Saccharomyces cerevisiae*. Microbiol Spectr. 2015 Apr;3(2):MDNA3–0053.

1308 83. Curcio MJ, Garfinkel DJ. Single-step selection for Ty1 element retrotransposition. Proc
1309 Natl Acad Sci USA. 1991 Feb 1;88(3):936–940.

1310 84. Behrens R, Hayles J, Nurse P. Fission yeast retrotransposon Tf1 integration is targeted
1311 to 5' ends of open reading frames. Nucleic Acids Res. 2000 Dec 1;28(23):4709–4716.

1312 85. Singleton TL, Levin HL. A long terminal repeat retrotransposon of fission yeast has strong
1313 preferences for specific sites of insertion. Eukaryotic Cell. 2002 Feb;1(1):44–55.

1314 86. Tsukahara S, Bousios A, Perez-Roman E, Yamaguchi S, Leduque B, Nakano A, et al.
1315 Centrophilic retrotransposon integration via CENH3 chromatin in *Arabidopsis*. Nature.
1316 2025 Jan 1;637(8046):744–748.

1317 87. Dai J, Xie W, Brady TL, Gao J, Voytas DF. Phosphorylation regulates integration of the
1318 yeast Ty5 retrotransposon into heterochromatin. Mol Cell. 2007 Jul 20;27(2):289–299.

1319 88. Cordaux R, Batzer MA. The impact of retrotransposons on human genome evolution. Nat
1320 Rev Genet. 2009 Oct;10(10):691–703.

1321 89. Thomas J, Vadnagara K, Pritham EJ. DINE-1, the highest copy number repeats in
1322 Drosophila melanogaster are non-autonomous endonuclease-encoding rolling-circle
1323 transposable elements (Helentrons). Mob DNA. 2014 Jun 4;5:18.

1324 90. Feschotte C, Jiang N, Wessler SR. Plant transposable elements: where genetics meets
1325 genomics. Nat Rev Genet. 2002 May;3(5):329–341.

1326 91. Cavrak VV, Lettner N, Jamge S, Kosarewicz A, Bayer LM, Mittelsten Scheid O. How a
1327 retrotransposon exploits the plant's heat stress response for its activation. PLoS Genet.
1328 2014 Jan 30;10(1):e1004115.

1329 92. Pietzenuk B, Markus C, Gaubert H, Bagwan N, Merotto A, Bucher E, et al. Recurrent
1330 evolution of heat-responsiveness in *Brassicaceae* COPIA elements. Genome Biol. 2016
1331 Oct 11;17(1):209.

1332 93. Garrigues JM, Tsu BV, Daugherty MD, Pasquinelli AE. Diversification of the
1333 *Caenorhabditis* heat shock response by Helitron transposable elements. Elife. 2019 Dec
1334 11;8.

1335 94. Lawler JF, Haeusser DP, Dull A, Boeke JD, Keeney JB. Ty1 defect in proteolysis at high
1336 temperature. J Virol. 2002 May;76(9):4233–4240.

1337 95. Cappucci U, Noro F, Casale AM, Fanti L, Berloco M, Alagia AA, et al. The Hsp70
1338 chaperone is a major player in stress-induced transposable element activation. Proc Natl
1339 Acad Sci USA. 2019 Sep 3;116(36):17943–17950.

1340 96. Yadav V, Mohan R, Sun S, Heitman J. Calcineurin contributes to RNAi-mediated
1341 transgene silencing and small interfering RNA production in the human fungal pathogen
1342 *Cryptococcus neoformans*. Genetics. 2024 Jan 27;

1343 97. Kiełbowicz-Matuk A, Smaczniak C, Mikołajczak K, Kuczyńska A, Xu X, Braeuning C, et
1344 al. Heat stress causes chromatin accessibility and related gene expression changes in
1345 crown tissues of barley (*Hordeum vulgare*). Plant Mol Biol. 2024 Oct 22;114(6):115.

1346 98. Huang Y, An J, Sircar S, Bergis C, Lopes CD, He X, et al. HSFA1a modulates plant heat
1347 stress responses and alters the 3D chromatin organization of enhancer-promoter
1348 interactions. Nat Commun. 2023 Jan 28;14(1):469.

1349 99. Hall BM, Ma C-X, Liang P, Singh KK. Fluctuation analysis CalculatOR: a web tool for the
1350 determination of mutation rate using Luria-Delbruck fluctuation analysis. Bioinformatics.
1351 2009 Jun 15;25(12):1564–1565.

1352 100. Hommelsheim CM, Frantzeskakis L, Huang M, Ülker B. PCR amplification of repetitive
1353 DNA: a limitation to genome editing technologies and many other applications. Sci Rep.
1354 2014 May 23;4:5052.

1355 101. Blum M, Andreeva A, Florentino LC, Chuguransky SR, Grego T, Hobbs E, et al. InterPro:
1356 the protein sequence classification resource in 2025. Nucleic Acids Res. 2025 Jan
1357 6;53(D1):D444–D456.

1358 102. Hum YF, Jinks-Robertson S. DNA strand-exchange patterns associated with double-
1359 strand break-induced and spontaneous mitotic crossovers in *Saccharomyces cerevisiae*.
1360 PLoS Genet. 2018 Mar 26;14(3):e1007302.

1361 103. Moore A, Dominska M, Greenwell P, Aksenova AY, Mirkin S, Petes T. Genetic control of
1362 genomic alterations induced in yeast by interstitial telomeric sequences. Genetics. 2018
1363 Jun;209(2):425–438.

1364 104. Tamura K, Stecher G, Kumar S. MEGA11: Molecular Evolutionary Genetics Analysis
1365 version 11. Mol Biol Evol. 2021 Jun 25;38(7):3022–3027.

1366 105. Pitkin JW, Panaccione DG, Walton JD. A putative cyclic peptide efflux pump encoded by
1367 the *TOXA* gene of the plant-pathogenic fungus *Cochliobolus carbonum*. Microbiology
1368 (Reading, Engl). 1996 Jun;142 (Pt 6):1557–1565.

1369 106. Koren S, Walenz BP, Berlin K, Miller JR, Bergman NH, Phillippy AM. Canu: scalable and
1370 accurate long-read assembly via adaptive k-mer weighting and repeat separation.
1371 Genome Res. 2017 May;27(5):722–736.

1372 107. Kolmogorov M, Yuan J, Lin Y, Pevzner PA. Assembly of long, error-prone reads using
1373 repeat graphs. Nat Biotechnol. 2019 May;37(5):540–546.

1374 108. Li H. Minimap2: pairwise alignment for nucleotide sequences. Bioinformatics. 2018 Sep
1375 15;34(18):3094–3100.

1376 109. Langmead B, Salzberg SL. Fast gapped-read alignment with Bowtie 2. Nat Methods.
1377 2012 Mar 4;9(4):357–359.

1378 110. Walker BJ, Abeel T, Shea T, Priest M, Abouelliel A, Sakthikumar S, et al. Pilon: an
1379 integrated tool for comprehensive microbial variant detection and genome assembly
1380 improvement. PLoS One. 2014 Nov 19;9(11):e112963.

1381 111. Robinson JT, Thorvaldsdóttir H, Winckler W, Guttman M, Lander ES, Getz G, et al.
1382 Integrative genomics viewer. Nat Biotechnol. 2011 Jan;29(1):24–26.

1383 112. Janbon G, Ormerod KL, Paulet D, Byrnes EJ, Yadav V, Chatterjee G, et al. Analysis of
1384 the genome and transcriptome of *Cryptococcus neoformans* var. *grubii* reveals complex
1385 RNA expression and microevolution leading to virulence attenuation. PLoS Genet. 2014
1386 Apr 17;10(4):e1004261.

1387 113. Altschul SF, Gish W, Miller W, Myers EW, Lipman DJ. Basic local alignment search tool.
1388 J Mol Biol. 1990 Oct 5;215(3):403–410.

1389 114. Camacho C, Coulouris G, Avagyan V, Ma N, Papadopoulos J, Bealer K, et al. BLAST+:
1390 architecture and applications. BMC Bioinformatics. 2009 Dec 15;10:421.

1391 115. Goel M, Schneeberger K. plotsr: visualizing structural similarities and rearrangements
1392 between multiple genomes. Bioinformatics. 2022 May 13;38(10):2922–2926.

1393 116. Shumate A, Salzberg SL. Liftoff: accurate mapping of gene annotations. Bioinformatics.
1394 2021 Jul 19;37(12):1639–1643.

1395 117. Pedersen BS, Quinlan AR. Mosdepth: quick coverage calculation for genomes and
1396 exomes. Bioinformatics. 2018 Mar 1;34(5):867–868.

1397 118. Katoh K, Misawa K, Kuma K, Miyata T. MAFFT: A novel method for rapid multiple
1398 sequence alignment based on fast Fourier transform. Nucleic Acids Res. 2002 Jul
1399 15;30(14):3059–3066.

1400 119. Page AJ, Taylor B, Delaney AJ, Soares J, Seemann T, Keane JA, et al. SNP-sites: rapid
1401 efficient extraction of SNPs from multi-FASTA alignments. Microb Genom. 2016 Apr
1402 29;2(4):e000056.

1403 120. Cingolani P, Platts A, Wang LL, Coon M, Nguyen T, Wang L, et al. A program for
1404 annotating and predicting the effects of single nucleotide polymorphisms, SnpEff: SNPs
1405 in the genome of *Drosophila melanogaster* strain w1118; iso-2; iso-3. Fly (Austin). 2012
1406 Jun;6(2):80–92.

1407

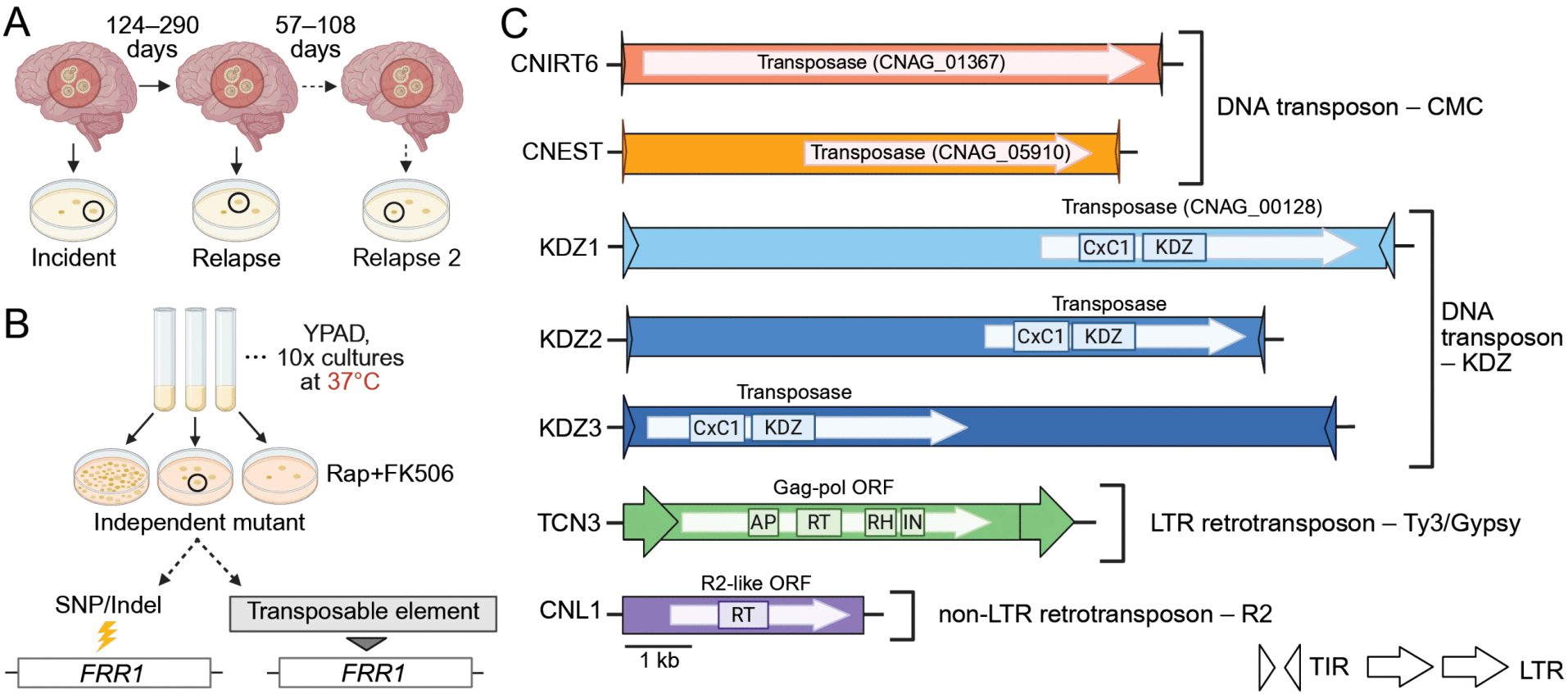

Fig 1. Diverse transposable elements (TEs) captured mobilizing in clinical isolates of *C. neoformans*. (**A**) Schematic of clinical isolate collection from patients with recurrent cryptococcal meningitis at disease onset and after subsequent relapse(s). Single colonies were isolated from patient cerebrospinal fluid on non-selective medium [55]. (**B**) Diagram of the preliminary screen using the "transposon trap" assay. Isolates were cultured in non-selective liquid YPAD medium at 37°C and plated on medium containing rapamycin and FK506 (rap+FK506) (N = 10 per isolate). Point mutations or TE insertions in the ~934 bp *FRR1* (CNAG_03682) reporter gene confer resistance to rap+FK506. (**C**) Illustration of seven mobile TEs detected in *C. neoformans* isolates, including DNA transposons from the CMC (CACTA, Mirage, Chapaev) supergroup and KDZ (Kyakuja/Dileera/Zisupton) superfamily, and retrotransposons from the Ty3/gypsy and R2 superfamilies. Terminal inverted repeats (TIRs) and long terminal repeats (LTRs) are indicated by triangles and arrows, respectively. Genes within TEs that are predicted to facilitate mobilization are shown as white arrows. Functional domains are indicated, including KDZ (Kyakuja/Dileera/Zisupton transposase), CxC1 (predicted zinc chelating domain), AP (aspartic protease), RT (reverse transcriptase), RH (RNase H), and IN (integrase). TEs are drawn to scale. Created in BioRender. Gusa, A. (2025) https://BioRender.com/1psvbhx.

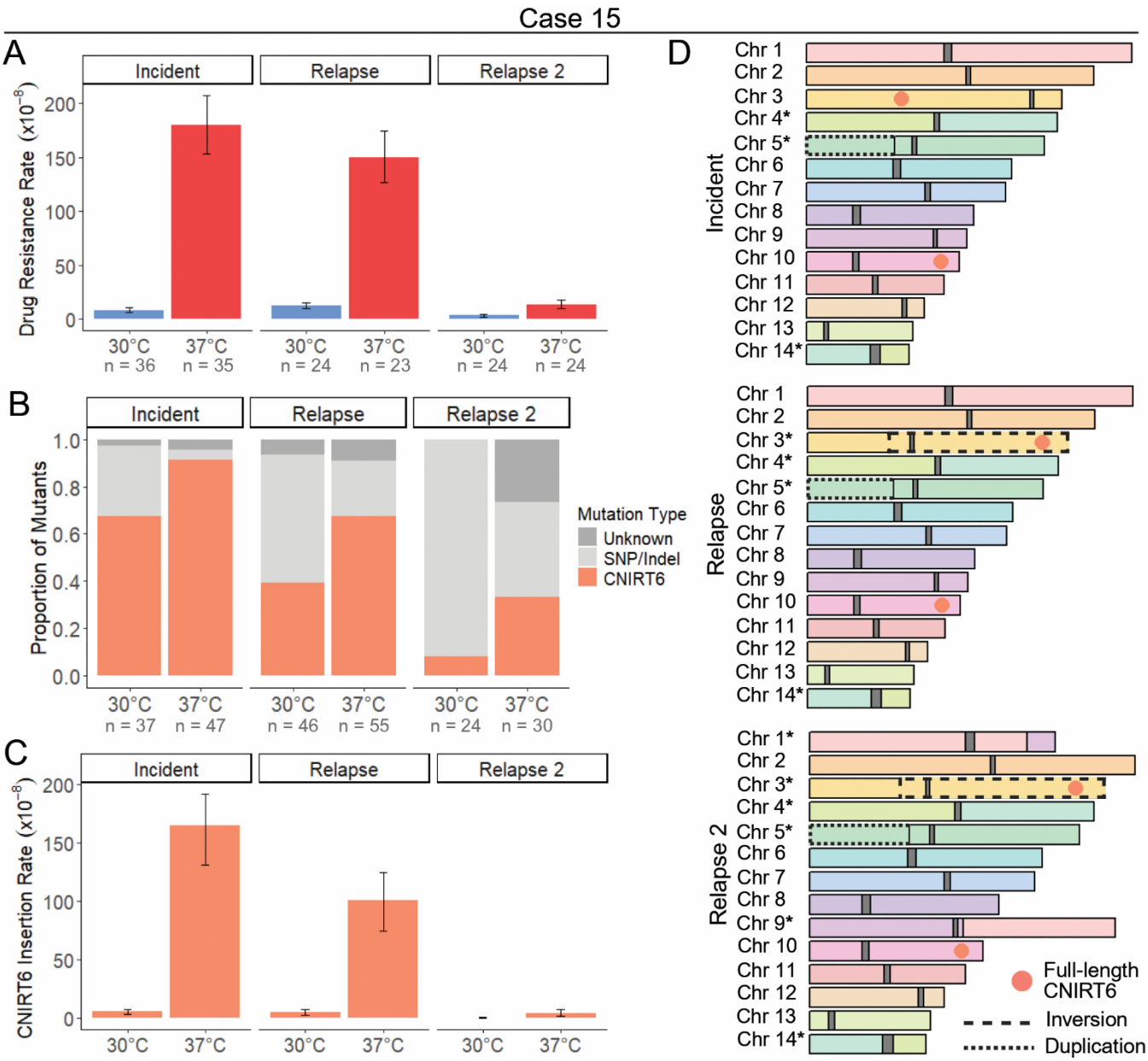

Fig 2. Mobilization of the DNA transposon CNIRT6 is induced by heat stress. (**A**) Rap+FK506 drug resistance rates per cell per generation following growth in non-selective YPAD medium at 30°C or 37°C (N = 23 – 36). (**B**) Mutation spectra in the *FRR1* gene for independent rap+FK506-resistant mutants. The mutation type "Unknown" indicates failure to amplify *FRR1* or absence of detectable mutations in its sequence (N = 24 – 55). (**C**) Insertion rate of CNIRT6 into *FRR1* per cell per generation. (**D**) Chromosome maps of the wild-type case 15 incident, relapse, and relapse 2 isolates. Full-length copies of CNIRT6 are shown as orange circles, and centromeres are shown as dark gray blocks. Chromosome synteny is indicated by chromosome color, with inversions and duplications outlined in dashed and dotted lines, respectively. All chromosomes with identified structural rearrangements are marked with an asterisk. Error bars in (**A**) and (**C**) represent 95% confidence intervals (CIs); rates are considered statistically different if error bars do not overlap.

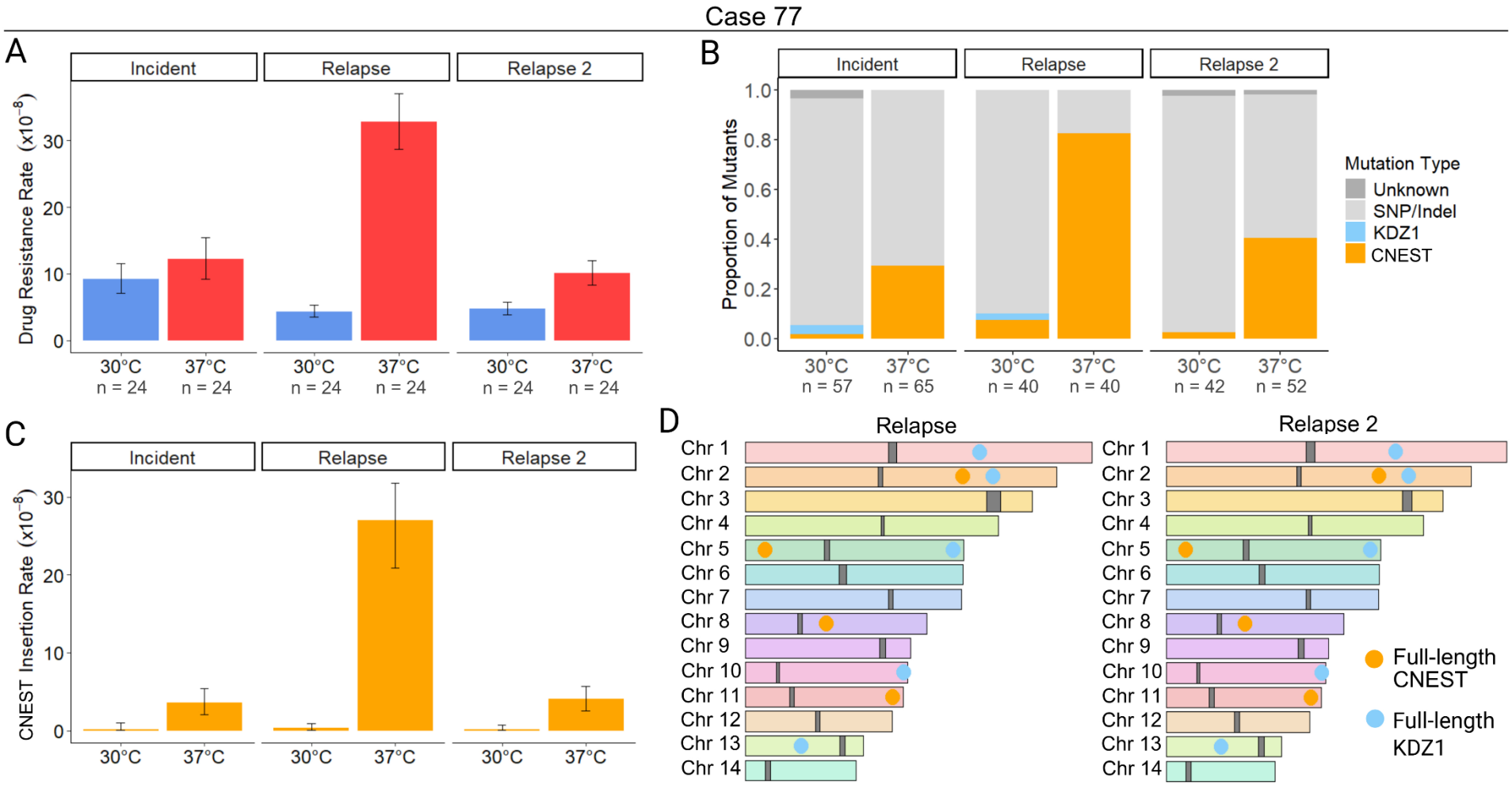

Fig 3. Mobilization of the DNA transposon CNEST is induced by heat stress. (**A**) Rap+FK506 drug resistance rates per cell per generation following growth in non-selective YPAD medium at 30°C or 37°C (N = 24). (**B**) Mutation spectra in the *FRR1* gene for independent rap+FK506-resistant mutants. The mutation type "Unknown" indicates failure to amplify *FRR1* or absence of detectable mutations in its sequence (N = 40 – 65). (**C**) Insertion rate of CNEST into *FRR1* per cell per generation. (**D**) Chromosome maps of the wild-type case 77 relapse and relapse 2 isolates. Full-length copies of CNEST (gold) and KDZ1 (light blue) are shown as circles, and centromeres are shown as dark gray blocks. Chromosome synteny is indicated by chromosome color. Error bars in (**A**) and (**C**) represent 95% confidence intervals (CIs); rates are considered statistically different if error bars do not overlap.

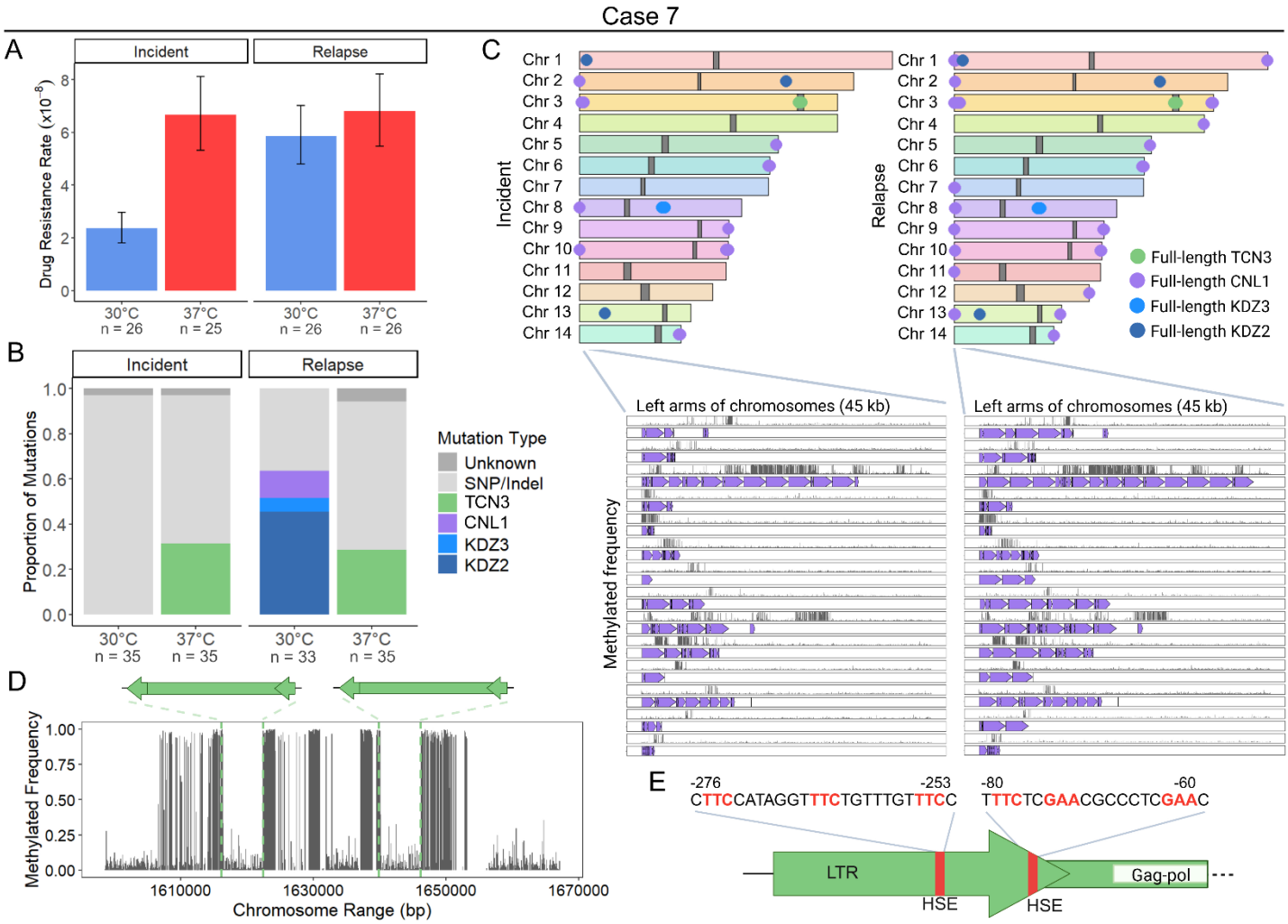

Fig 4. Temperature- and strain-specific TE dynamics in case 7. (**A**) Rap+FK506 drug resistance rates per cell per generation following growth in non-selective YPAD medium at 30°C or 37°C (N = 25 – 26). (**B**) Mutation spectra in the *FRR1* gene for independent rap+FK506-resistant mutants. The mutation type "Unknown" indicates failure to amplify *FRR1* or absence of detectable mutations in its sequence (N = 33 – 35). (**C**) Chromosome maps of the wild-type case 7 incident and relapse isolates. Full-length copies of TCN3 (green), CNL1 (purple), KDZ3 (blue), and KDZ2 (dark blue) are shown as circles, and centromeres are shown as dark gray blocks. Chromosome synteny is indicated by chromosome color. Insets show the 45 kb regions on the left arms of chromosomes in the incident and relapse isolates. Purple arrows indicate all CNL1 BLASTn hits; grey lines represent DNA methylation frequency from long reads, with the y-axis scaled from 0 to 1. (**D**) DNA methylation frequency plotted for the Chr 3 centromere region ±10 kb of the incident isolate. The position and orientation of full-length TCN3 copies is shown. (**E**) Diagram of HSE sequence motifs (red) identified in TCN3 LTRs. Position is shown relative to the gag-pol open reading frame (ORF) translation start site. Created in BioRender. Gusa, A. (2025) https://BioRender.com/ucajfxd.

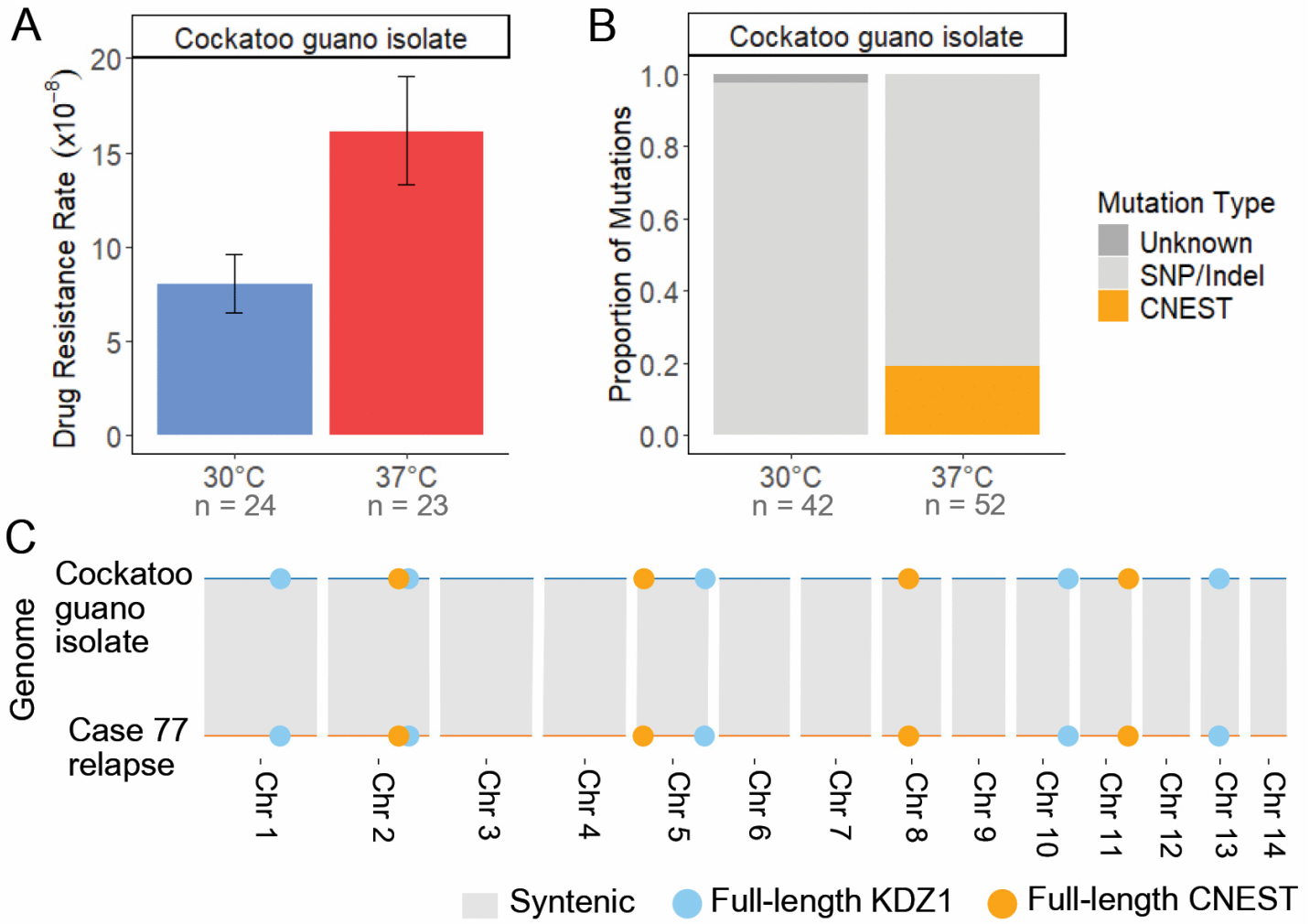

Fig 5. Heat stress-induced CNEST activation is conserved in an environmental isolate. (**A**) Rap+FK506 drug resistance rates per cell per generation following growth in non-selective YPAD medium at 30°C or 37°C (N = 23 – 24). Error bars represent 95% confidence intervals (CIs); rates are considered statistically different if error bars do not overlap. (**B**) Mutation spectra in the *FRR1* gene for independent rap+FK506-resistant mutants. The mutation type "Unknown" indicates failure to amplify *FRR1* or absence of detectable mutations in its sequence (N = 42 – 52). (**C**) Chromosome-level synteny between the cockatoo guano and case 77 relapse isolates. Full-length copies of CNEST (gold) and KDZ1 (light blue) are shown as circles.

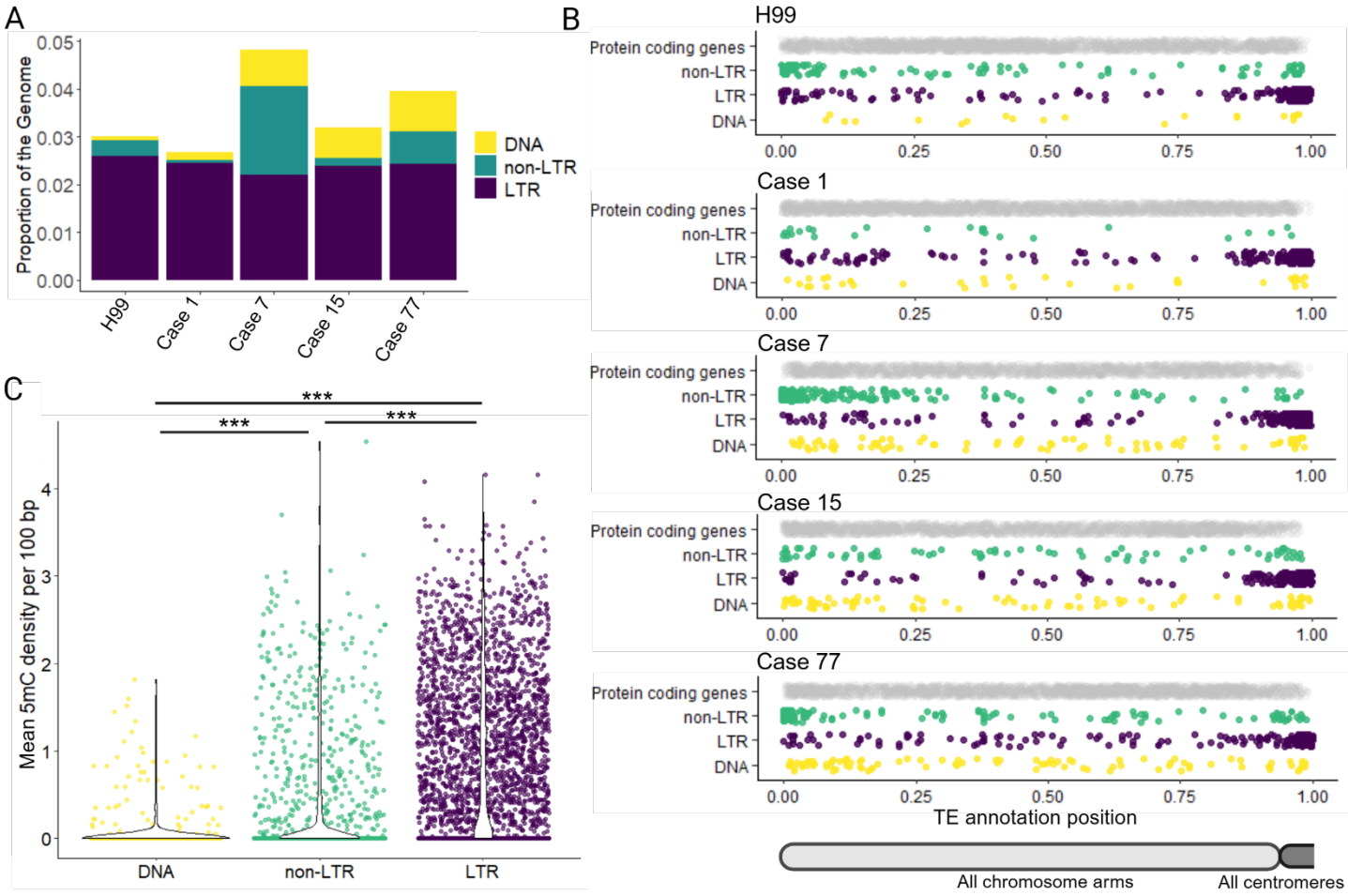

Fig 6. Genomic distribution and DNA methylation differ among non-LTR, LTR, and DNA transposons. (**A**) The proportion of the genome composed of non-LTR, LTR, and DNA transposons, based on Earl Grey TE annotations. (**B**) Scaled positions of protein coding genes and non-LTR, LTR, and DNA transposons across chromosome arms. Chromosomes were split at the midpoint of the centromere region, and protein-coding gene and TE positions were scaled from 0 to 1 based on chromosome arm length. Data for all chromosome arms is plotted. (**C**) Mean 5mC DNA methylation density per 100 bp for DNA, non-LTR, and LTR TEs in isolates from cases 1, 7, 15, and 77. Violin plots are overlaid to illustrate the distribution. Significance was assessed using the pairwise Wilcoxon rank-sum test with continuity correction. *** denotes Bonferroni-adjusted $p < 2e\text{-}16$. The first genome assembly from serially collected clinical isolates was chosen as a representative for all cases in (**A**), (**B**), and (**C**).

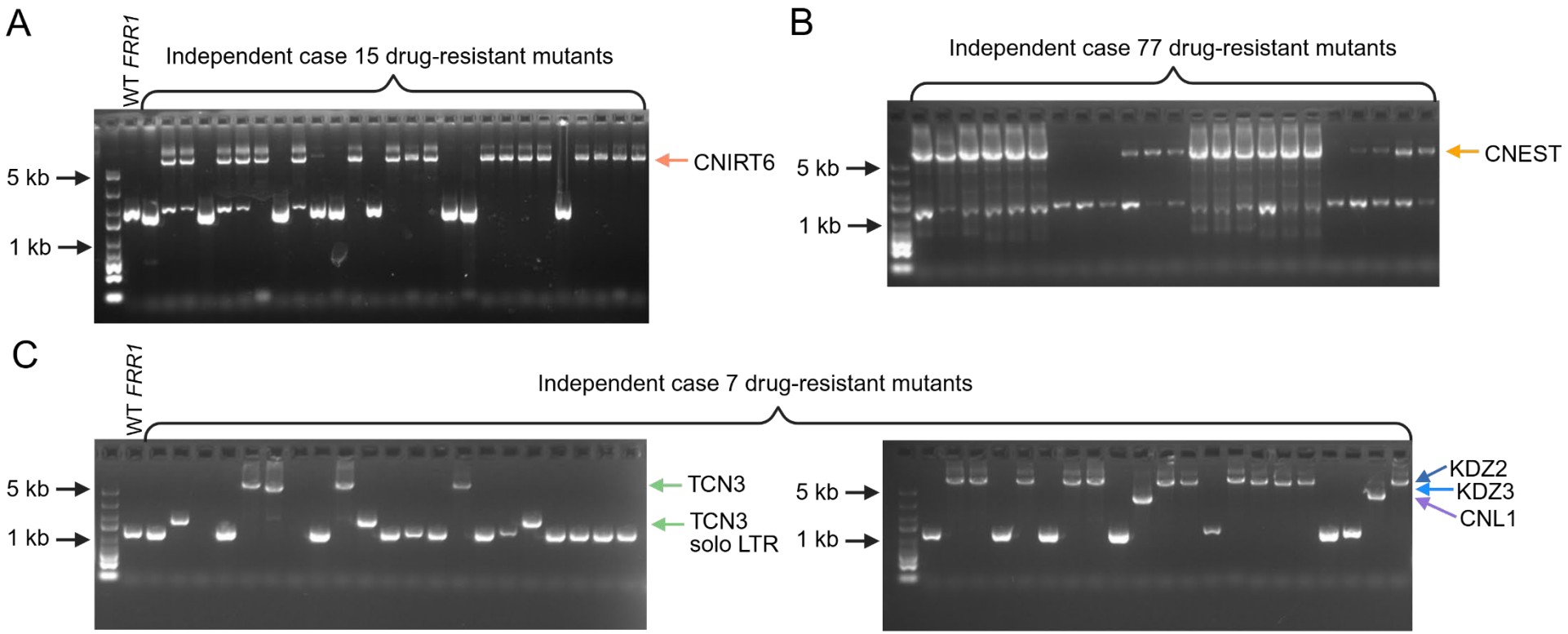

Fig S1. PCR amplification of *FRR1* in wild-type and independent rap+FK506-resistant mutants. *FRR1* was amplified from independent drug-resistant mutants from case 15 (**A**), case 77 (**B**), and case 7 (**C**); a subset of representative mutants are shown. Higher molecular weight bands indicative of TE insertion in *FRR1* were verified by Sanger or linear amplicon sequencing, or junction PCR. Colored arrows indicate the molecular weights of bands identified as TEs.

A

```
cttgtccgtc acccctttcc ggagcggagg acctgcaata ctttccattc   60
ttctttcttc ttcttcATGT TCAGATCTAT CCTCACCACC TCTCGCCCCC  120
TCGTTAGACA GCCTCTCCGT CAATTTACTA CAACAGCTAT CAAAATGGGT  180
GTTACTGTTG AGgttggtat cttctgcttt ctcctagtga ccgatcggtc  240
cggagtgcat ctgagcgtca gtgctgatat gttgactgat ttttcttgcc  300
ttcaacagAA CATTTCCGCC GGTGACGGCA AGACCTTCCC CCAGCCTGGA  360
GACAATGTTA CTATCCACTg tgggttgtcc ttaaactccg cttcctgtgc  420
atctcgagat gagaacttgc aacactgaca tgatggcgac cttttgctat  480
gtaaatagAC GTTGGTACCC TTCTTGACGG TTCCAAGTTT GACTCTTCCC  540
GAGACCGTGG AACGCCCTTC GTCTGCCGAA TTGGCCAAGG gtaagtattt  600
ccgaaggtgc gcatatttca tagctgatac tgtttcgtag CCAAGTTATC  660
AGGGGTTGGG ACGAGGGTGT TCCTCAGCTC TCCGTAGGCC AGAAGGCTAA  720
CCTCATCTGT ACCCCTGACT ATGgtatgcg aagtttcttt cgttgcaaca  780
aattaaacct gacatctatc aattagCCTA CGGTGCGCGA GGTTTCCCCC  840
CTGTTATTCC TCCCAACTCC ACCCTCAAGT TCGAGGgtaa gtttgctctt  900
cgtcgacact acgtacctga cactgatttt tattacagTT GAGCTCCTCA  960
AGGTCAACTA AAatttattg cgtaaattag tagatggtct taaaagttag 1020
gaaatctgaa tgataagtga aagaagaatt aagtagacga tgatatgaac 1080
ggtgtggcga atgcttctaa acgtttcaaa attg
```

CNIRT6

B

CNIRT6 Insertion	TSD	Size of TSD
1	TAG	3
2	CGA	3
3	CTG	3
4	TAT	3
5	TTG	3
6	CAG	3
7	TTA	3

Fig S2. CNIRT6 insertion into *FRR1*. (**A**) A subset of CNIRT6 insertion sites (orange arrows) mapped in *FRR1*. The 5′ and 3′ untranslated regions (UTRs) of *FRR1* are underlined; introns are shown in lowercase, exons in capital letters, and the start codon is bolded. (**B**) TSDs detected at CNIRT6 insertion sites. Insertions are ordered based on their appearance in the *FRR1* sequence from beginning to end.

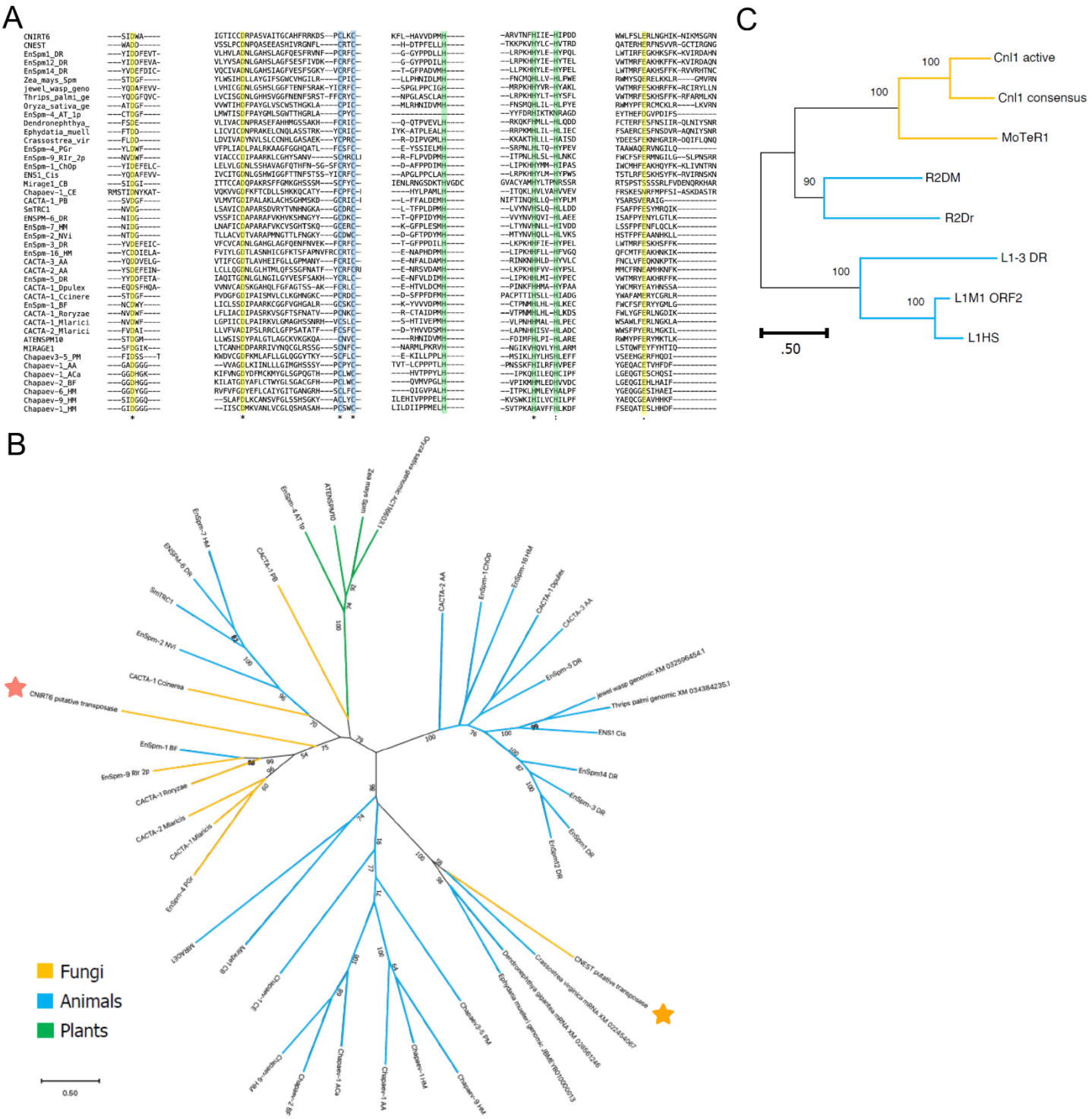

Fig S3. Classification of CNIRT6, CNEST, and CNL1. (**A**) Regions of interest in a multiple sequence alignment highlighting conserved residues in CMC supergroup elements, which include members of the CACTA (also known as EnSpm), Mirage, and Chapaev superfamilies. Highlighted residues include the DDE catalytic core (yellow), conserved cysteine residues (blue) and conserved histidine residues (green) [41]. (**B**) Unrooted amino acid phylogeny of diverse CMC transposases, demonstrating the relationship of CNIRT6 and CNEST with known CMC families and other related sequences. CNIRT6 is marked with an orange star, and CNEST with a gold star. (**C**) Unrooted amino acid phylogeny of reverse transcriptase domains, demonstrating the relationship between CNL1 and MoTeR1, and more distantly related R2 elements from flies and fish, as well as mammalian L1 elements. Branches in (**B**) and (**C**) are colored by kingdom: animals (blue), plants (green), and fungi (yellow). Bootstrap values greater than 50% are shown at nodes. Scale bars represent amino acid substitutions per site. Abbreviations: HS – *Homo sapiens*, DR – *Danio rerio*, DM – *Drosophila melanogaster*, CE – *Caenorhabditis elegans,* CB – *Caenorhabditis briggsae*, PM – *Petromyzon marinus*, BF – *Branchiostoma floridae*, Dpulex – *Daphnia pulex*, Cis – *Ciona intestinalis*, Aca – *Aplysia californica*, Sm – *Schistosoma mansoni*, AA – *Aedes aegypti*, ChOp – *Chionoecetes opilio*, Jewel wasp/NVi – *Nasonia vitripennis*, HM – *Hydra magnipapillata*, Ccinerea – *Coprinopsis cinerea*, RIr – *Rhizophagus irregularis*, Roryzae – *Rhizopus oryzae*, Mlaricis – *Melampsora laricis*, PGr – *Puccinia graminis*, PB – *Phycomyces blakesleeanus*, Mo – *Magnaporthe oryzae*, AT – *Arabidopsis thaliana*.

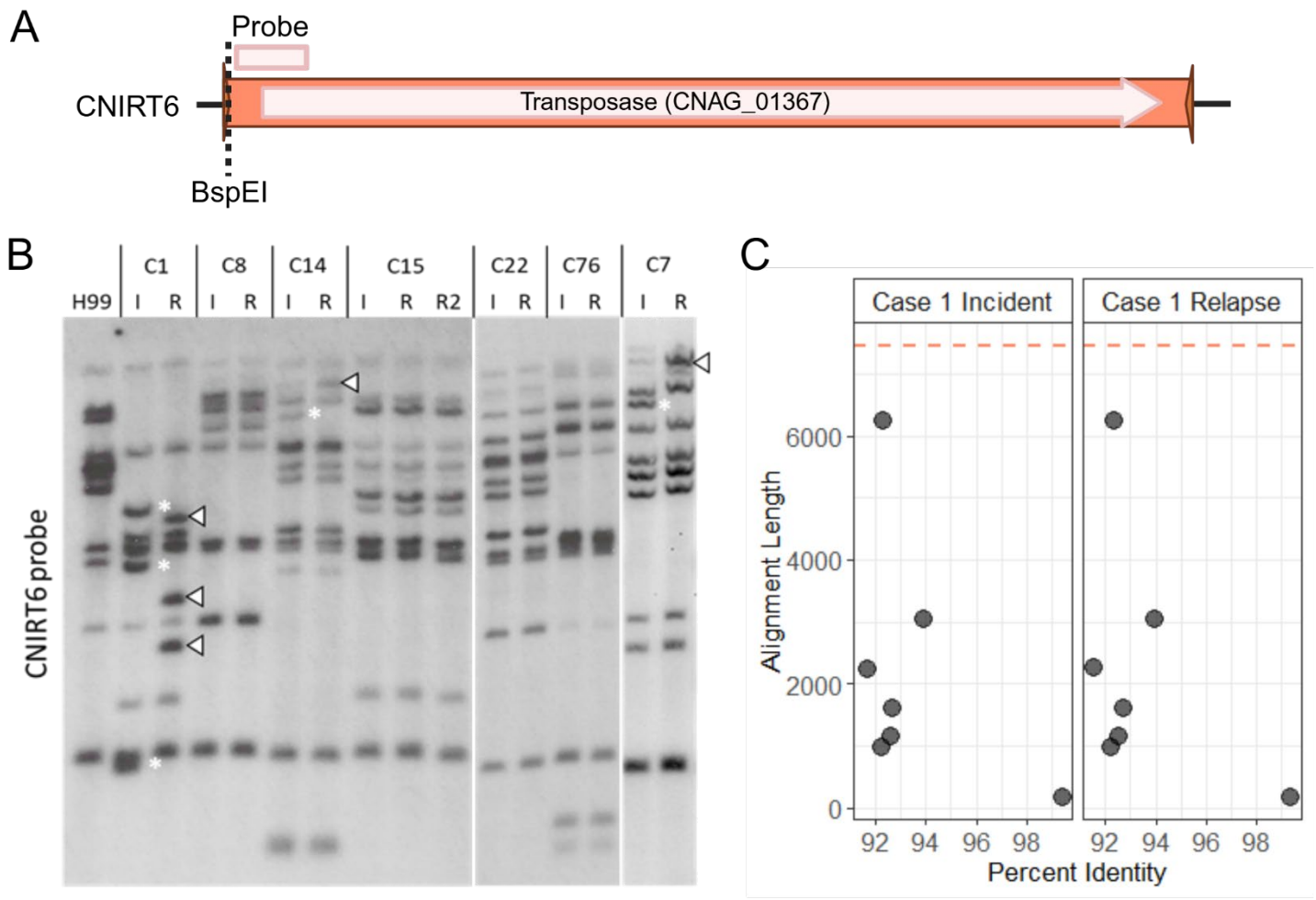

Fig S4. Putative CNIRT6 transposition events in serially collected clinical isolates. (**A**) Location of the restriction site (dotted line) and CNIRT6-specific probe used in Southern analysis. (**B**) Southern blot of genomic DNA digested with BspEI probed for CNIRT6 in incident (I) and relapse (R) isolates; case numbers are indicated as C#. Asterisks denote the loss of CNIRT6 fragments, while arrowheads indicate the emergence of CNIRT6 fragments at new genomic locations between incident and relapse isolates. (**C**) BLAT homology search hits identified in case 1 isolates using full-length CNIRT6 as the query. The orange dashed line indicates the length of full-length CNIRT6.

A

```
ctcgtccgtc acccctttcc ggagcggagg acctgcaata ctttccattc   60
ttctttcttc ttcttcATGT TCAGATCTAT CCTCACCACC TCTCGCCCCC  120
TCGTTAGACA GCCTCTCCGT CAATTTACTA CAACAGCTAT CAAAATGGGT  180
GTTACTGTTG AGgtcggtat cttctgcttt ctccttagtg accgatcggt  240
ccggagtgca tctgagcgtc agtgctgata tgttgactga tttttcttgc  300
cttcaacagA ACATTTCCGC CGGTGACGGC AAGACCTTCC CCCAGCCTGG  360
AGACAATGTT ACTATCCACT gtgggttgtc cttaaactcc acttcctgtg  420
catctcgaga tgagaacttg caacactgac atgatggcga ccttttgcta  480
tgtaaatagA CGTTGGTACC CTTCTTGACG GTTCCAAGTT TGACTCTTCC  540
CGAGACCGTG GAACTCCCTT CGTCTGCCGA ATTGGCCAAG Ggtaagtatt  600
tccgaaggtg cgcgtacttc attagctgat actgtttcgt agCCAAGTTA  660
TCAGGGGTTG GGACGAGGGT GTTCCTCAGC TCTCCGTAGG CCAGAAGGCT  720
TAACCTCGTC TGTACCCCTG ACTACGgtat gcgaagtttc tttcgttgca  780
acaaattaaa cctgacatct atcaattagC CTACGGTGCG CGAGGTTTCC  840
CCCCTGTTAT CCCCCCCAAC TCCACCCTCA AGTTCGAGGg taagtttgct  900
cttcgtcgac actacgtacc tgacactgat ttttattaca gTTGAGCTCC  960
TCAAGGTCAA CTAAaatttt ttgcgtaaat tagtagatgg tcttaaaagt 1020
taggaaatct gaatgatagt ggaagaagaa ttaagtagac gatgatatga 1080
acggtgtggc gaatgcttct aaatgtttca aaattgcatt gct        1140
```

B

CNEST Insertion	TSD	Size of TSD
1	TA	2
2	TA	2
3	TA	2
4	TA	2
5	TA	2
6	TA	2
7	TA	2
8	TA	2
9	TA	2
10	TA	2
11	TA	2
12	TA	2

KDZ1 Insertion	TSD	Size of TSD
1	GAGCGTCA	8

CNEST
KDZ1

Fig S5. CNEST and KDZ1 insertion into *FRR1*. (**A**) A subset of CNEST (gold) and KDZ1 (light blue) insertion sites are mapped with arrows in *FRR1*. The 5′ and 3′ UTRs of *FRR1* are underlined; introns are shown in lowercase, exons in capital letters, and the start codon is bolded. (**B**) TSDs detected at CNEST and KDZ1 insertion sites. Insertions are ordered based on their appearance in the *FRR1* sequence from beginning to end.

A

```
ctcgtccgtc acccctttcc ggagcggagg acctgcaata ctttccattc   60
ttctttcttc ttcttcATGT TCAGATCTAT CCTCACCACC TCTCGCCCCC  120
TCGTTAGACA GCCTCTCCGT CAATTTACTA CAACAGCTAT CAAAATGGGT  180
GTTACTGTTG AGgttggtat cttctgcttt ctccttagtg accgatcggt  240
ccggagtgca tctgagcgtc agtgctgata tgttgactga tttttcttcc  300
cttcaacagA ACATTTCCGC CGGTGACGGC AAGACCTTCC CCCAGCCTGG  360
AGACAATGTT ACTATCCACT gtgggttgtc cttaaactcc gcttcctgtg  420
catctcgaga tgagaacttg caacactgac atgatggcga ccttttgcta  480
tgtaaatagA CGTTGGTACC CTTCTTGACG GTTCCAAGTT TGACTCTTCC  540
CGAGACCGTG GAACTCCCTT CGTCTGCCGA ATTGGCCAAG Ggtaagtatt  600
tccgaaggtg cgcatatttc atagctgata ctgtttcgta gCCAAGTTAT  660
CAGGGGTTGG GACGAGGGTG TTCCTCAGCT CTCCGTAGGC CAGAAGGCTA  720
ACCTCATCTG TACCCCTGAC TATGgtatgc gaagtttctt tcgttgcaac  780
aaattaaacc tgacatctat caattagCCT ACGGTGCGCG AGGTTTCCCC  840
CCTGTTATTC CCCCCAACTC CACCCTCAAG TTCGAGGgta agtttgctct  900
tcgtcgacac tacgtacctg acactgattt ttattacagT TGAGCTCCTC  960
AAGGTCAACT AAaatttatt gcgtaaatta gtagatggtc ttaaaagtta 1020
ggaaatctga atgatagtga aagaagaatt aagtagacga tgatatgaac 1080
ggtgtagcga atgcttctaa atgtttcaaa attg
```

KDZ2
KDZ3
CNL1
TCN3

B

KDZ2 Insertion	TSD	Size of TSD
1	GCTTTCTC	8
2	CCTTAGTG	8
3	CCGA	4
4	CCGGAGTG	8
5	CAGTGCTG	8
6	AGTTATCA	8
7	GGGACGAG	8
8	GGTGTTCC	8
9	CAATTAGC	8
10	CTCAAGTT	8

KDZ3 Insertion	TSD	Size of TSD
1	CGGTCCGG	8
2	CCGGAGTG	8
3	TCTGAGCG	8
4	CAAGGGTA	8
5	TAGCTGAT	8
6	GCTGATAC	8
7	AAGTTATC	8
8	GTTGGGAC	8
9	TCTGTACC	8
10	GACA	4

CNL1 Insertion	TSD	Size of TSD
1	CA	2
2	A	1
3		0
4	CACC	4
5	CACCCCT	7
6	CACCCCTTTCC	11
7	CACCCCTTTCCGG	13
8		0
9	ATCAGGGGT	9

TCN3 Insertion	TSD	Size of TSD
1	CTGAG	5
2	TGTTG	5
3	TGTTG	5
4	TTTGC	5
5	GTTTC	5
6	TTATC	5
7	GGGTG	5
8	GCTAA	5
9	CCTAC	5
10	GAGGG	5

Fig S6. KDZ2, KDZ3, CNL1, and TCN3 insertion into *FRR1*. (**A**) A subset of KDZ2 (dark blue), KDZ3 (blue), CNL1 (purple), and TCN3 (green) insertion sites are mapped with arrows in *FRR1*. The 5′ and 3′ UTRs of *FRR1* are underlined; introns are shown in lowercase, exons in capital letters, and the start codon is bolded. (**B**) TSDs detected at KDZ2, KDZ3, CNL1, and TCN3 insertion sites. Insertions are ordered based on their appearance in the *FRR1* sequence from beginning to end.

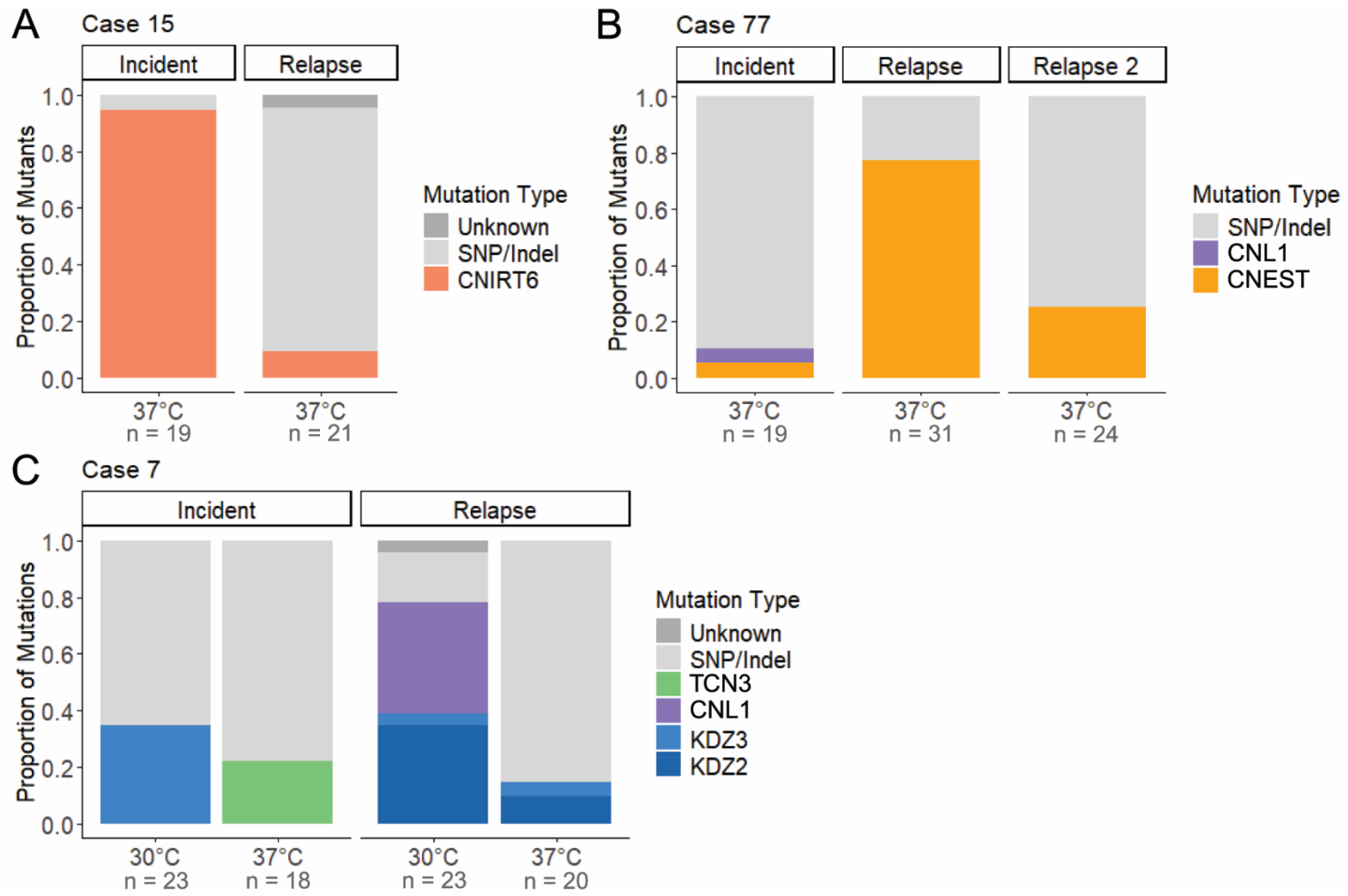

Fig S7. Growth in RPMI medium alters TE mobilization dynamics. Mutation spectra in the *FRR1* gene for independent rap+FK506-resistant mutants in case 15 (**A**), case 77 (**B**), and case 7 (**C**). The mutation type "Unknown" indicates failure to amplify *FRR1* or absence of detectable mutations in its sequence (N = 18 – 31).

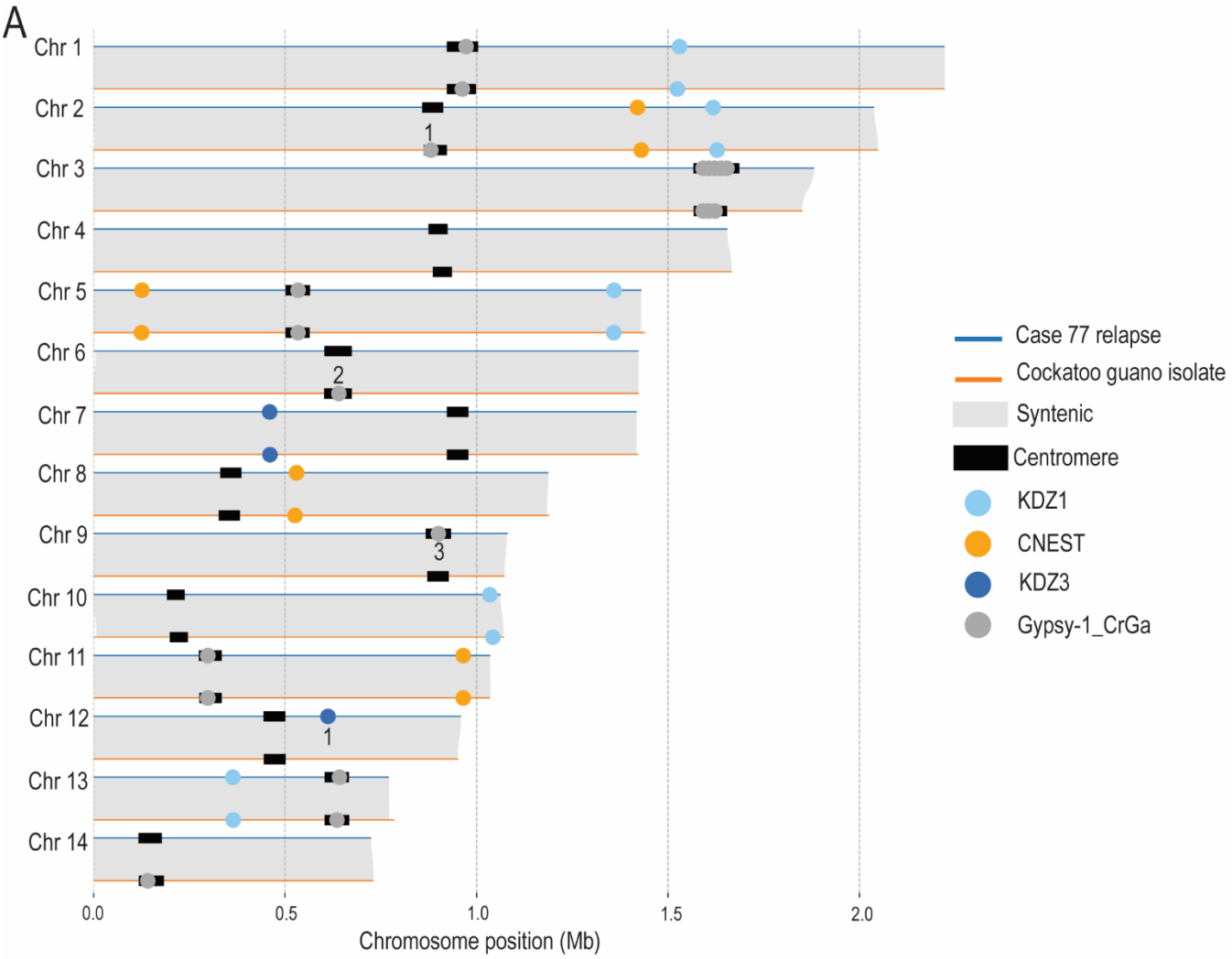

B

Insertion	TSD	Size of TSD (bp)
KDZ3 1	GAATGGAT	8
Gypsy-1_CrGa 1	TGCCTC	6
Gypsy-1_CrGa 2	TGACTG	6
Gypsy-1_CrGa 3	GCTAAC	6

Fig S8. Transposition events between the cockatoo guano and case 77 relapse isolates. (**A**) Chromosome-level synteny between the case 77 relapse and cockatoo guano isolates. Full-length copies of CNEST (gold), KDZ1 (light blue), KDZ3 (dark blue), and Gypsy-1_CrGa (dark grey) are shown as circles. Predicted centromere regions are indicated by black rectangles and detected transposition events are numbered. (**B**) TSDs detected at KDZ3 and Gypsy-1_CrGa insertion sites.

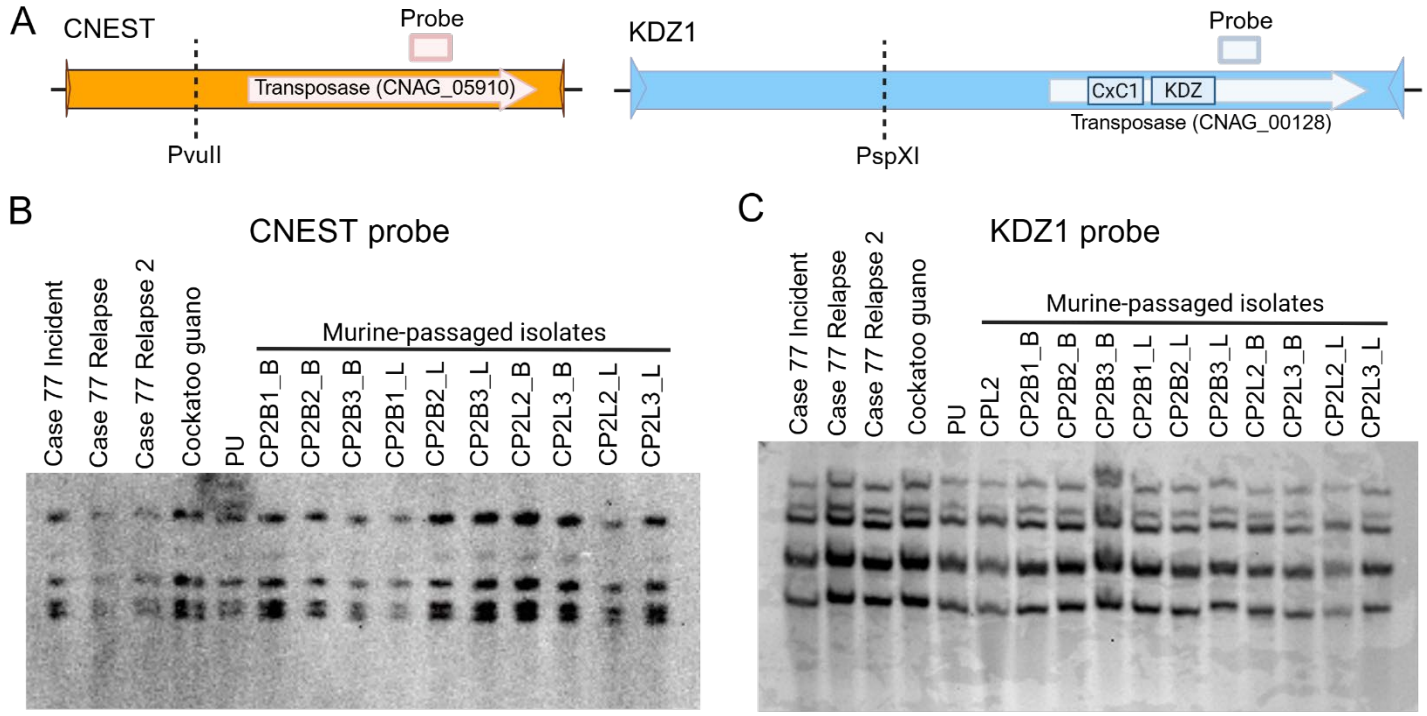

Fig S9. No predicted transposition of CNEST or KDZ1 in murine-passaged isolates. (**A**) Location of the restriction sites (dotted lines) and CNEST- and KDZ1-specific probes used in the Southern analysis. Southern blots of (**B**) PvuII-digested genomic DNA probed for CNEST, and (**C**) PspXI-digested genomic DNA probed for KDZ1. Shown are case 77 isolates, the cockatoo guano isolate, the patient isolate (PU) infected by the guano point-source strain, and cockatoo guano isolates passaged one to two times through mice by Sephton-Clark et al. (2023), recovered from brain or lung tissue (see Table S1 for strain details).

A

	CNIRT6	CNEST	KDZ1	KDZ2	KDZ3	CNL1	TCN3	Gypsy-1_CaGr
Case 1 Incident	0	1	0	0	0	0	1	1
Case 1 Relapse	0	1	0	0	0	0	1	2
Case 7 Incident	0	1	1	3	2	16	2	12
Case 7 Relapse	0	1	1	3	2	39	2	12
Case 15 Incident	2	1	0	0	0	0	1	1
Case 15 Relapse	2	1	0	0	0	0	1	1
Case 15 Relapse 2	2	1	0	0	0	0	1	1
Case 77 Relapse	0	4	5	0	2	0	0	11
Case 77 Relapse 2	0	4	5	0	2	0	0	8
Cockatoo guano	0	4	5	0	1	0	0	11
H99	2	2	1	0	0	0	1	3

B

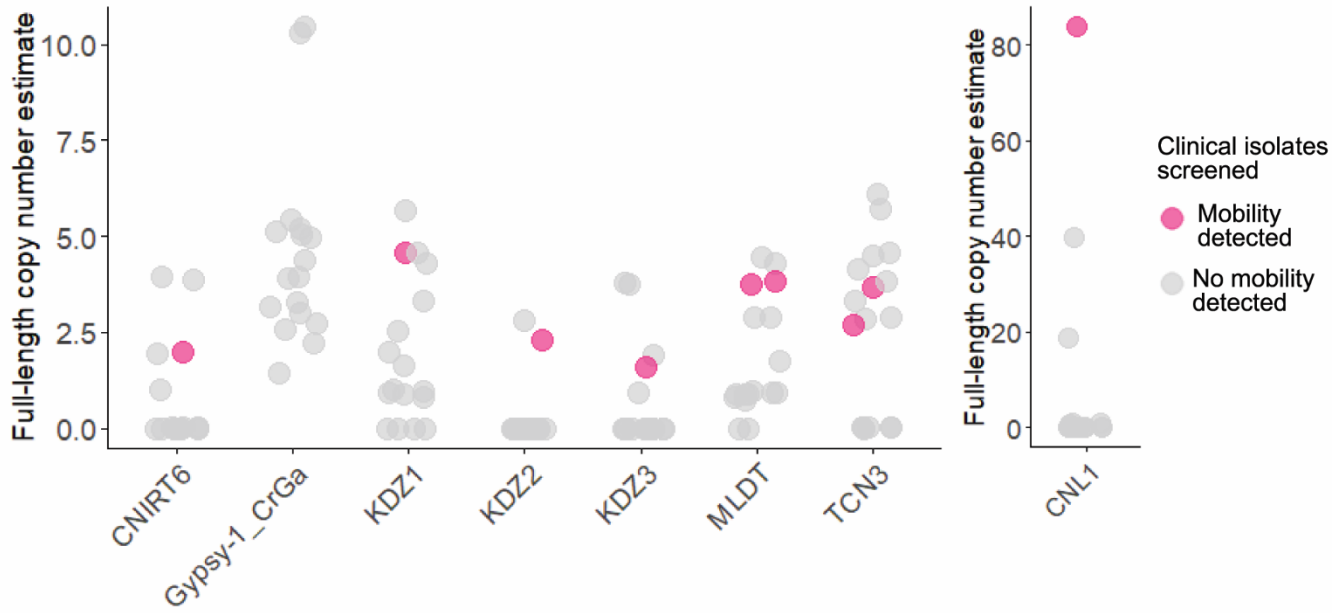

Fig S10. Full-length TE copies are present in genomes where no in vitro mobilization was detected. (**A**) Full-length TE copy numbers identified in whole-genome assemblies using BLAT and BLASTn homology searches. TE copy numbers in isolates with observed mobilization events into *FRR1* in YPAD medium are highlighted in pink. Isolate names are colored by lineage: VNI (blue), VNII (green), and VNBII (orange). (**B**) Full-length TE copy number estimates from short-read sequencing for all 15 *C. neoformans* incident isolates screened, except for case 7, where both incident and relapse isolates are shown. Isolates with no insertions into *FRR1* in YPAD medium are shown in grey, and those with insertions are shown in pink.

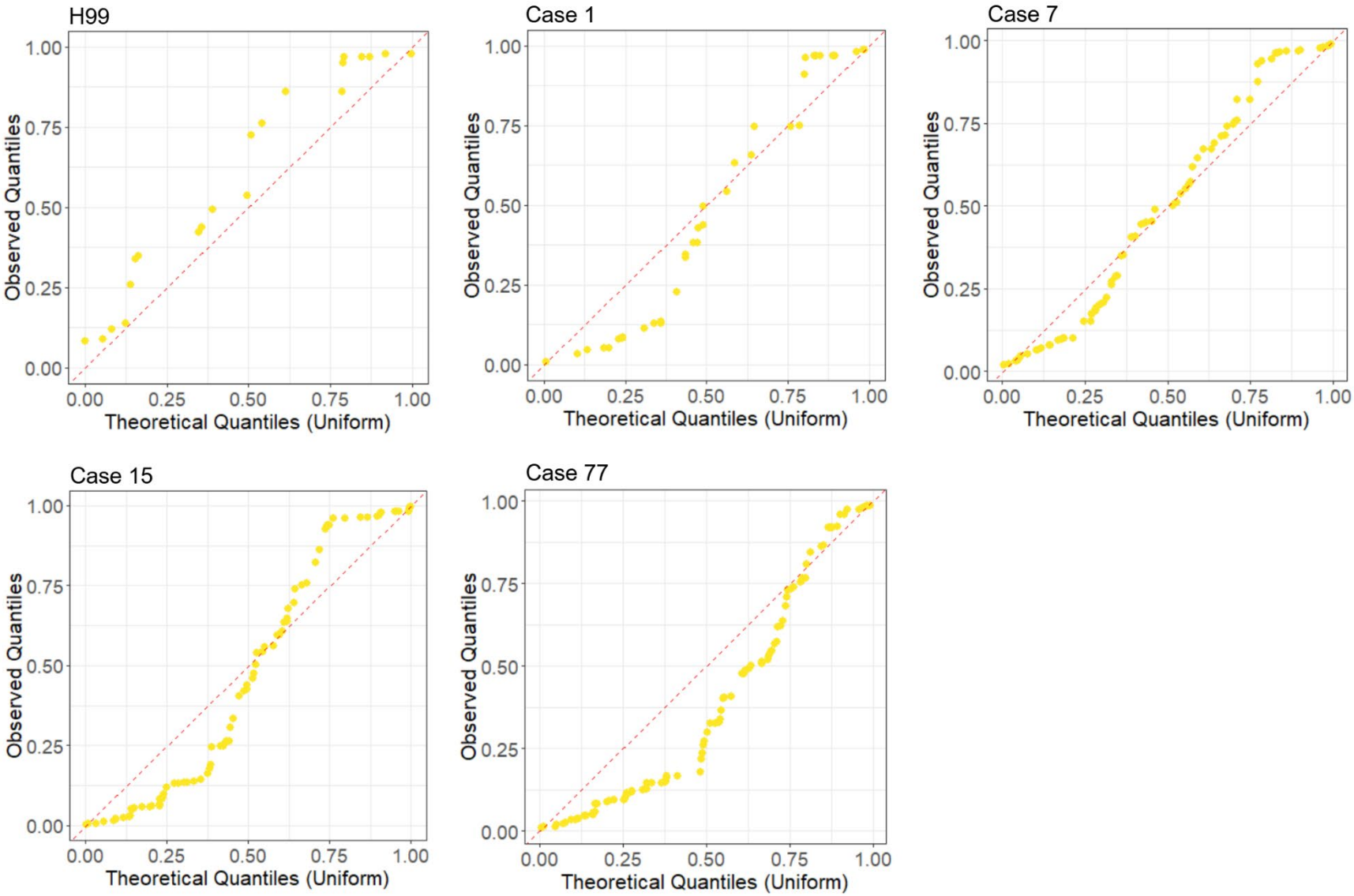

Fig S11. DNA TEs are approximately uniformly distributed across the genome. Quantile-quantile (QQ) plots are shown for the H99 reference genome and the first genome assembly from serially collected clinical isolates for cases 1, 7, 15, and 77 (representative examples). Observed quantiles correspond to the scaled positions (0 to 1) of DNA TEs along all chromosome arms. Theoretical quantiles are uniformly distributed random values between 0 and 1, sorted in ascending order, with their total number matching the number of observed DNA TEs.

A

Transposon type	Isolate	Total annotations	Percent methylated
LTR	Case 1	370	62.7
	Case 7	350	64.0
	Case 15	336	71.1
	Case 77	281	55.9
	Median	**343**	**63.4**
non-LTR	Case 1	25	8.0
	Case 7	223	53.4
	Case 15	74	8.1
	Case 77	204	37.7
	Median	**139**	**22.9**
DNA	Case 1	36	8.3
	Case 7	84	7.1
	Case 15	84	15.5
	Case 77	95	8.4
	Median	**84**	**8.4**

B

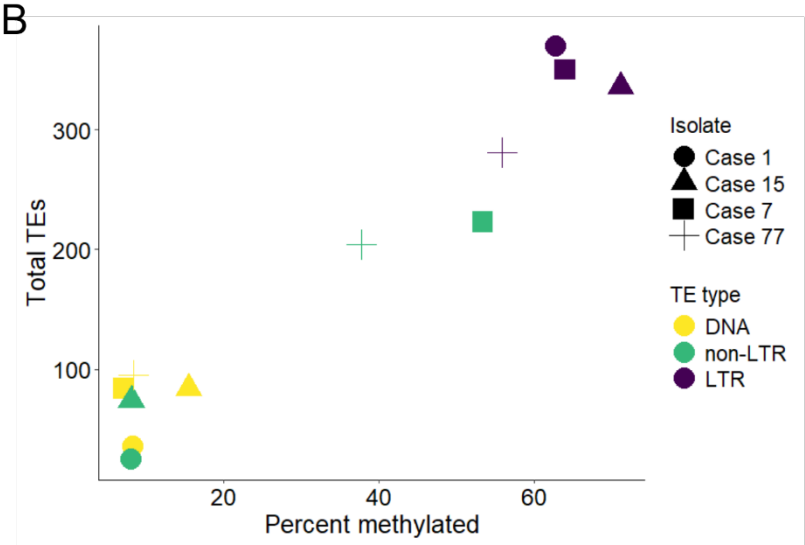

Fig S12. DNA transposons are less frequently methylated than LTR and non-LTR retrotransposons. (**A**) Number of TEs per type and the percentage containing at least one high-confidence DNA methylation call (methylation frequency > 0.75), with median values shown. (**B**) TE types (colors) per genome (shapes) and the percentage with at least one high-confidence DNA methylation call (methylation frequency > 0.75). The first genome assembly from serially collected clinical isolates was chosen as a representative.

Table S1. Strains used in this study.

Table S2. Transposable elements characterized in this study.

Table S3. Whole-genome sequencing and assemblies used in this study.

Table S4. DNA methylation analysis of full-length transposable element copies.

Table S5. Primers used in this study.